



School of Chemistry

**Construction and Operation of a Plasma System to
Fluorinate and Aminate the Surfaces of Diamond
Thin Films**

By: Tarik Al-Jeda

**Thesis submitted on the 13th of April 2018 in partial fulfilment for the
Honours degree of MSci Chemistry at the University of Bristol**

Supervisor: Professor Paul May
Second Assessor: Dr. Neil Fox
Physical and Theoretical

Abstract

The ability to terminate the diamond surface with different atoms/molecules has allowed for an emergence of new biological and technological applications. H-terminated diamond is the most common form for synthetic chemical vapour deposition (CVD) diamond and exhibits surface conductivity and a negative electron affinity (NEA). Through the use of either wet or dry chemical methods the surface bonds can be changed from C-H to C-O, C-X (halogen) or C-N. These terminations result in changes in the electron affinity, stability of nitrogen vacancies and hydrophobicity of the diamond sample.

This project focused on the construction of a plasma reactor in order to perform fluorine and ammonia termination of high pressure high temperature (HPHT) diamond samples, provided by Element Six.

Following the construction of the reactor, optical emission spectroscopy was used to identify the species that were generated by the plasma. For the NH₃ reactor transitions relating to the NH species and H atoms were found, whilst for the SF₆ reactor the predominant species were F and SF₆.

Contact angle measurements were performed on the newly terminated diamond surfaces in order to measure the degree of termination as a function of time. This allowed for the determination of an ideal plasma exposure time, 20 s for F-termination and 120 s for NH₃-termination.

X-ray photoelectron spectroscopy (XPS) was used to confirm the presence of amine species on the diamond surface, through the N1s binding energy region between 396-403 eV. Two components were found to make up this peak. They represented the imine (398 eV) and secondary amine (400 eV) bonding environment. XPS also showed that after 30 s there was a plateau in the maximum percentage of nitrogen on the surface, 40%. Moreover, the XPS data suggested that an increased exposure to the ammonia plasma resulted in a preference for imines over secondary amine groups.

Scanning electron microscopy (SEM) was used to identify etching on the F-terminated diamond surface. The images showed regions of varied etching. Backscattered SEM also suggested the presence of another heavier element on the diamond surface that could potentially be fluorine. However further XPS analysis is needed to confirm this.

Acknowledgments

I would like to thank both Dr. James Smith and Ed Aldred for helping with the construction of the reactor and getting me started on the road to becoming a certified plumber. Thanks also to Fabian Fogarty for helping me with the NanoESCA and collecting XPS data. I would like to extend my gratitude to Michael and Alex who helped me with hydrogen terminations throughout the year. A special thank you to Afaq whose guidance and support from day one helped make this project so fun to work on.

Thanks also to Professor Paul May whose reassurance helped ease the initial panic at the start of the project. Also thank you to Dr. Neil Fox who offered innovative ways to go about analysing the surface.

Additionally I would like to thank my parents whose reassurance helped me get through the project with most of my sanity intact. I would also like to thank my grandma whose constant nagging kept me focused on the important tasks at hand.

1. Table of Contents

2. List of Figures	7
3. List of Tables	9
4. Introduction	10
4.1 History and Properties of Diamonds	10
4.2 Diamond Synthesis	11
4.3 High Pressure High Temperature Synthesis	11
4.4 Chemical Vapour Deposition	13
4.4.1 Nucleation and Seeding	13
4.4.2 CVD Reaction Chamber	14
4.4.3 Gas Phase Reactions	15
4.4.4 Diamond Growth	16
4.5 Doping.....	19
4.6 Diamond Surface	20
4.6.1 (111) Surface	21
4.6.2 (100) Surface	22
4.6.3 Surface Roughness.....	23
4.7 Surface Terminations	24
4.8 Hydrogen Terminated Diamond	24
4.8.1 Surface Structure	24
4.8.2 Methods for Hydrogen Terminating Diamond	24
4.8.3 Surface Conductivity	25
4.8.4 Negative Electron Affinity and Secondary Electron Yields	26
4.8.5 Hydrophobicity	27
4.9 Oxygen Terminated Diamond	28
4.9.1 Surface Structure	28
4.9.2 Methods for Oxidizing Diamond	29
4.9.3 Properties of Oxygen Terminated Diamond	31

4.10 Fluorine Terminated Diamond	32
4.10.1 Surface Structure.....	32
4.10.2 Methods of Fluorinating Diamond.....	33
4.10.3 Properties and Uses of Fluorine Terminated Diamond.....	33
4.11 Nitrogen/Ammonia Terminated Diamond	35
4.11.1 Nitrogen Terminated Diamond Surface.....	35
4.11.2 Methods for Achieving Nitrogen/Ammonia Terminated Diamond	35
4.11.3 Application of Ammonia Terminated Diamond	36
4.12 Plasma Termination	37
4.13 Alternative Functionalization Methods	38
4.13.1 Surface Functionalization	38
4.13.2 Photolithography.....	40
5. Material Preparation and Experimental Techniques.....	41
5.1 Project Aim	41
5.2 Sample Preparation	41
5.2.1HPHT Diamond	41
5.2.2 Acid Clean	41
5.2.3 Boron Doping	42
5.2.4 Hydrogen Termination.....	43
5.3 Plasma Reactor.....	44
5.3.1 Construction of a Plasma Reactor.....	44
5.3.2 Gases Chosen for Terminations	46
5.3.3 Standard Operation of the Plasma Reactor	47
5.4 Emission Spectroscopy	48
5.5 Analysis of Functionalized Surfaces.....	48
5.5.1 Wettability	58
5.5.2 Contact Angle Measurements	50
5.5.3 XPS	51

5.5.4 SEM	53
6. Results and Discussion.....	56
6.1 OES	56
6.2 Analysis of Functionalized Surfaces.....	57
6.2.1 Ammonia Termination.....	57
6.2.2 Fluorine Termination	58
6.2.3 Comparison of Contact Angle Measurements	60
6.3 XPS	61
6.3.1 Ammonia Termination.....	61
6.4 SEM	68
7. Conclusions.....	73
8. Further Work.....	75
9. References.....	76

2. List of Figures

Figure 1: Phase Diagram of Carbon ⁶	12
Figure 2: Effect of filament temperature on the deposits prepared at 1100 K under 37 Torr CH ₄ (1%)-H ₂ (a)-(c) and at 1150 K under 10 Torr CH ₃ (3%)-H ₂ (c), (d). Filament temperatures are (a) 2100 K C, (b) 2300 K (d) 2400 K (d) 2100 K (e), 2250 K (f) 2400 K. ¹⁷	14
Figure 3: Diagram of the band gap in a p-type semiconductor.....	19
Figure 4: Diagram of the band gap in an n-type semiconductor.....	20
Figure 5: A line graph that shows the different growth rates of the CVD diamond surface in different methane concentrations ²⁸	21
Figure 6: A side view of the models of diamond. The surfaces from right to left are: (111)- 1 x 1, (111) -2 x 1, (110) – 1 x 1, (100) 1 x 1 and (100) – 2 x 1 ²⁹	21
Figure 7: Pandey π bonded chain model of the (111) diamond surface.....	22
Figure 8: Surface produced by scaife polishing. The imaging was done through the use of atomic force microscopy. The grooves on the surface are < 5nm nm wide.....	23
Figure 9: 2 x 1:H structure of the (100) diamond surface. Here the structure is composed of monohydride dimers where each dangling bond is terminated by hydrogen ³⁸	24
Figure 10: Increased surface roughness of type Ib HPHT diamonds due to exposure to hydrogen plasma ⁴¹	25
Figure 11: Band structure of diamond close to the surface. Here sub-bands are formed just below the conduction band just above the valence band ⁴³	26
Figure 12: Partial dissociation of the ozone molecule on the diamond surface ⁵⁷	29
Figure 13: Complete dissociation of the ozone molecule on the diamond surface ⁵⁷	30
Figure 14: Oxidation reactions on a diamond surface at increasing temperatures. These reactions took place in an atmosphere of 20% O ₂ /Ar ⁶⁰	30
Figure 15: Reaction a takes place in 10% Cl ₂ /90% Ar ₂ atmosphere. Between 500 and 700 K. Reaction b took place in air where water vapour reacted with the surface to produce the hydroxyl and ether groups. In reaction c diamond was heated while exposed to air resulting in the formation of the ketone group instead of the hydroxyl ⁶¹	31
Figure 16: Energy band diagrams of full hydrogenated, partially hydrogenated and oxygenated diamond. Here we can see how oxygen termination causes surface band bending ⁶⁴	32
Figure 17: Nitrogen vacancy centre in the diamond lattice ⁷⁴	34
Figure 18: Attachment of Horseradish Enzyme onto diamond surface ⁷⁹	36
Figure 19: Illustration of TFAAD attached to diamond using a ball and stick model. Chain length was determined by Gaussian98 using B3LYP calculations ⁸²	37
Figure 20: Thiol functionalization steps ⁸⁶	39
Figure 21: Reduction of aryldiazonium salt and attachment of benzene ring onto the diamond surface.	39
Figure 22: SEM image of fluorine-terminated diamond with varying diameter in a surrounding oxygen terminated surface. The difference in surface conductivity allows for the visible difference ⁵ .	40
Figure 23: Schematic diagram of the HF reaction chamber used to Boron dope the diamond sample ⁴²	
Figure 24: Schematic diagram of the microwave CVD reactor ⁸⁸	43
Figure 25: Schematic diagram of the O-termination plasma reactor. The labelled components are as follows: 1- vacuum chamber; 2 – cathode; 3 - plasma shield; 4- diamond sample; 5 – anode; 6 – conducting copper plate; 7 – grounded pedestal; 8 – line to gas inlet; 9 – power source; 10 – vent to air; 11 – gas inlet; 12 – MFC for both Ar and O; 13 – valves for the Ar and O lines; 14 – gas cylinders; 15 – needle value; 16 – shut off valve; 17 – Leybold Trivac rotary pump	45

Figure 26: Image of the completed plasma reactor with the labelled changes	46
Figure 27: Schematic diagram that demonstrates Young's Equation ⁹²	49
Figure 28: Image of the contact angle measurement generated by the Krüss Drop Shape Analyser with the use of the Advance program.	50
Figure 29: (A) XPS spectra of clean (C) and oxidized (OX) diamond. The peak at roughly 550 eV in the oxidized graph indicates the increase in oxygen on the diamond surface. (B) represents the oxygen concentration on the two samples which was calculated from XPS ⁹⁶ . On the x axis AR, C and OX represent: as received, cleaned and oxidized respectively. The subsequent numbers refer to different annealing temperatures.....	52
Figure 30: Schematic diagram of a hemispherical analyser ⁹⁷	53
Figure 31: More electrons are reflected off the heavier Cu atom in backscattered SEM.	54
Figure 32: Photograph of the JEOL IT 300 SEM.	55
Figure 33: The change in contact angle with an increased exposure to the ammonia plasma.....	58
Figure 34: The change in contact angle with an increased exposure to the SF ₆ plasma	59
Figure 35: The contact angle of the hydrogen, oxygen, ammonia and fluorine-terminated diamond surfaces	60
Figure 36: Survey scan of the initial 2 min NH ₃ terminated sample.	61
Figure 37: N1s binding environment in the initial 2 min NH ₃ -terminated sample.....	62
Figure 38: C1s binding environment in the initial 2 min NH ₃ -terminated sample	63
Figure 39: O1s binding environment in the initial 2 min NH ₃ -terminated sample	64
Figure 40: Survey scan of a sample that was oxygen terminated and then exposed to an ammonia plasma for 2 mins.....	64
Figure 41 (a): Survey scan of the 1 min NH ₃ -terminated sample. Figure 41 (b): Survey scan of the 2 min NH ₃ -terminated sample.....	65
Figure 42(a): Survey scan of the 30 s NH ₃ -terminated diamond sample. Figure 42(b): Survey scan of the 3 min NH ₃ -terminated diamond sample.....	66
Figure 43: N1s binding environment in the 30 s (a) and 3 min (b) NH ₃ -terminated samples.	67
Figure 44: O1s binding environment in the 30 s and 3 min NH ₃ -terminated sample.....	67
Figure 45: A SEM image of the entire HPHT diamond surface taken with ×45 magnification.	68
Figure 46: A SEM image of the diamond surface taken with a ×1000 magnification.....	69
Figure 47: Image of how holes present on the surface can affect the shape of the water droplet.....	70
Figure 48 (a and b): Secondary electron and backscattered images of the same diamond surface at a magnification of ×1500.....	70
Figure 49 (a and b): Secondary electron and backscattered SEM images of the same diamond surface at a magnification of ×7000.	71

3. List of Tables

Table 1: The Properties and uses of Natural and Synthetic Diamond.....	10
Table 2: Typical conditions for diamond growth.....	15
Table 3: Expected or measured threshold energies for electron impact dissociation of SF ₆ into neutral species ⁹⁰	47
Table 4: Conditions for generating the O ₂ , NH ₃ and SF ₆ plasmas	47
Table 5: The experimental and literature values of the species observed by OES in the SF ₆ plasma..	56
Table 6: The experimental and literature value of the species observed by OES in the NH ₃ plasma..	56

4. Introduction

4.1 History and Properties of Diamonds

Diamonds were first mined in India around the 4th century BC. They played an important role in society and people believed wearing diamonds could bring about greater fortune and health. Alexander the Great brought diamonds out of India and into the Mediterranean and then, through trade, diamonds began to also appear throughout Western Europe and other parts of the world¹.

However, the history of the modern diamond only began to take shape with the discovery of mines in South Africa in the late 19th century. Following the discovery of diamond mines in Kimberly around 1868, South Africa has been the world's largest producer of diamonds. Since then the annual production of diamonds has increased one hundred fold².

The name diamond originates from the Greek '*adámas*', this roughly translates to unbreakable, which is an apt description of its properties. Diamond is the hardest known material and can only be scratched by other diamonds. It also demonstrates several other unique and desirable qualities which can be seen in table 1.

Properties	Value in Natural Diamond	Value in Synthetic Diamond	Use
High thermal conductivity	25 W/cm K	24 W/cm K	Integrated as a thermal management material
Hardness	10,000 kg/mm ²	10,000 kg/mm ²	Coating for cutting tools
Highest known Young's Modulus	1.22 GPa	10.50 GPa	Abrasive or erosion-resistant
Low thermal expansion	0.0000011 /K	0.000001 /K	Heat spreaders for high power devices
High transparency to infrared, visible and UV light			Window and lens material

Table 1: The Properties and uses of Natural and Synthetic Diamond

These properties arise from the small atomic radius and tetrahedral bond structure of carbon. An atomic radius of 0.77 Å allows carbon to form closely spaced lattice structures. Each one of the sp³ hybridized carbons combines with four other similarly hybridized atoms to give the macromolecular covalent structure³.

This tightly packed structure and strong bonding, along with its low photon scattering, is also responsible for diamond's high thermal conductivity⁴.

4.2 Diamond Synthesis

Since natural diamonds are available as lumps or rock their incorporation into devices which requires films/coatings has proven to be difficult. The synthetic diamond field was created in order to combat this issue. One of the main issues of producing diamond is that the most stable carbon allotrope at ambient room temperature and pressure is graphite. This is demonstrated by the phase diagram in figure 1.

Although the difference between the stable graphite and metastable diamond phase is only 0.02 eV per atom there exists a high energy barrier of 0.4 eV per atom⁵. Therefore large amounts of heat and pressure are required to convert the phases. This high energy barrier is also the reason that once diamond is formed it is stable. These extreme conditions required to form diamond are the reason that the gem can only be found in certain locations around the world, deep within the Earth's crust in the lithospheric mantle.

4.3 High Pressure High Temperature Synthesis

The first attempts at creating synthetic diamond were based around the idea of creating an environment where diamond is the most stable phase. Since diamond is the densest form of carbon it will be stable at high pressures, as shown by the phase diagram below.

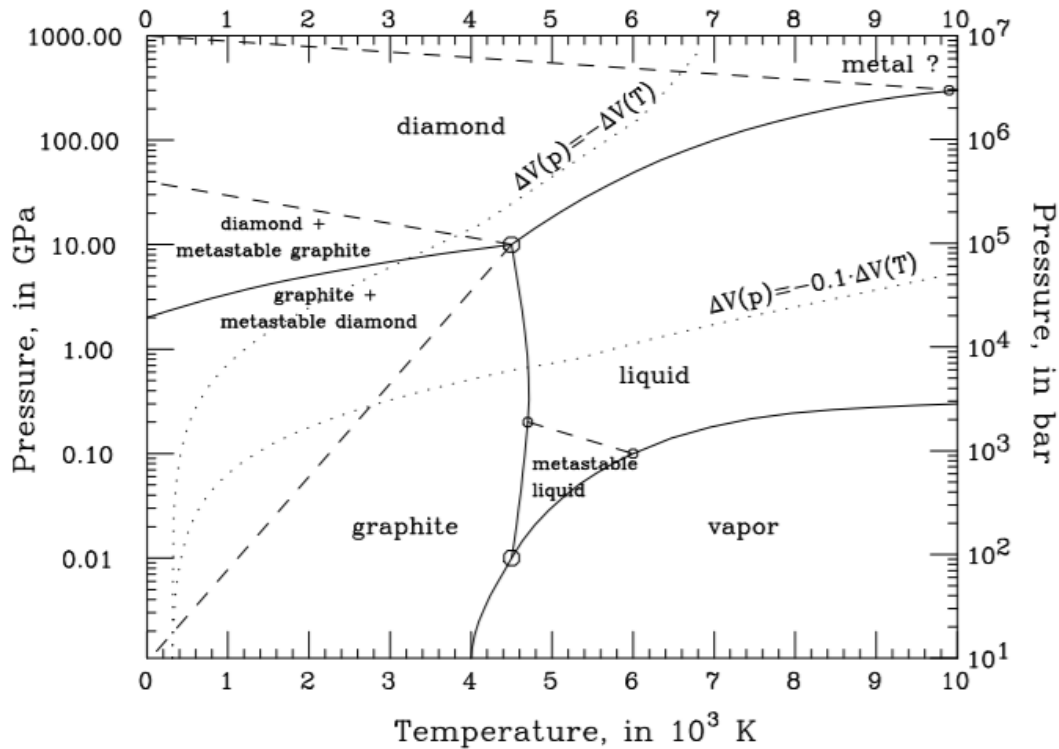


Figure 1: Phase Diagram of Carbon⁶

The first successful synthesis of diamond was based on this concept. It became known as the High Pressure High Temperature (HPHT) technique. First developed by General Electric in the 1950s, it involved heating graphite in solution to temperatures of around 2000 K at pressures of 10 GPa. The graphite was heated with nickel, cobalt and iron as solvent-catalysts. Following the initial heating the temperature was then lowered over time, thus reducing carbon solubility in the catalyst and resulting in the precipitation of excess carbon as diamond⁷. This method replicates the natural growing conditions where diamond forms at pressures of 5-6 GPa at temperatures between 1200-1500 K in non-metallic systems^{8,9,10}.

The apparatus used in the growth process contains a reaction cell which includes: graphite, diamond seed crystal and the solvent metal catalysts. As well as lowering the activation energy the metal catalysts also allow the solvation of carbon atoms in the graphite. Moreover it results in a temperature gradient being established between the diamond seed crystal and the graphite material. This in turn creates a carbon solubility difference that results in the precipitation of diamond. By using a small temperature gradient over extended growth times larger single crystal diamonds can be produced¹¹.

However, one of the main drawbacks is that this method produced diamonds in single crystal form, which limits its applications. Producing diamonds by HPHT is more complicated than the alternative chemical vapour deposition, however this issue is offset by the cheaper cost of production. This is the reason that HPHT still serves as the primary industrial method for producing synthetic diamonds¹².

HPHT diamond can come in a variety of different colours which is a result of impurities present during the growth process. The most common colour is the yellow-orange HPHT diamond which is due to the presence of isolated nitrogen atoms incorporated during the growth process. This results in n-type doping in the diamond.

The other common impurity present in the growth chamber is boron. This results in blue HPHT diamonds. Small amounts of boron causes the diamond to become a p-type semiconductor material, while heavily boron doped diamond usually demonstrates metallic behaviour¹³.

The pink coloured HPHT diamonds are a result of post growth treatment by irradiation and low temperature annealing. This process creates nitrogen vacancies (NV) which are responsible for the colour. Nitrogen vacancies are a point defect in the diamond lattice and will be discussed later in more detail¹⁴.

4.4 Chemical Vapour Deposition

An alternative to HPHT synthesis began to emerge in the 1950s, known as Chemical Vapour Deposition (CVD). This involves the addition of carbon atoms individually, from a hydrocarbon sub unit, onto a substrate. Initially diamond films were grown homoepitaxially, on natural diamond crystals. The growth was achieved by thermal decomposition of gases onto the substrate at temperatures of 1100 K. This produced poor quality films and also resulted in the co-deposition of graphite. The breakthrough came when USSR scientists found that hydrogen could etch and remove graphite to leave diamond. Unlike HPHT, CVD can grow nanocrystalline and polycrystalline diamonds¹⁵.

4.4.1 Nucleation and Seeding

Prior to the growth in the CVD reactor, nucleation must take place. This affects the film thickness, morphology and surface roughness. There are two different approaches to the nucleation processes, homogenous (gas phase) or heterogeneous (on the substrate). There have been only a few examples of homogenous nucleation succeeding, which therefore makes heterogeneous nucleation the preferred method.

Several different substrates can be used to grow diamond. Two of the most common substrates are silicon and molybdenum. Silicon is usually chosen over molybdenum as the substrate, due to the fact that it has a similar thermal expansion coefficient and lattice structure to diamond. This results in highly orientated crystal films. Moreover, use of silicon is cheaper than the homoepitaxial diamond alternative. Despite the similar thermal properties and lattice structure, nucleation on the silicon substrate still requires activation. This is because the nucleation density of silicon is only 10^4 nuclei/cm² whereas, the ideal nucleation density should be 10^8 nuclei / cm².¹⁶

Activation can be accomplished through scratching, substrate seeding or carburization of the substrate. One of the most common techniques is seeding. This involves the seeding of the substrate surface with submicron diamond powder. This in turn provides nucleation sites that allow the diamond film to grow. Furthermore, during this process, the seeding also causes the surface to be scratched which further enhances diamond growth rate.

Following seeding, CVD diamond growth can begin in the reaction chamber. There are three main steps to this, activation of the gas mixture, gas-phase reactions and diffusion of gas species onto the substrate.

4.4.2 CVD Reaction Chamber

CVD reactors work by activation of gaseous reactants above a substrate. In this case the gases are CH_4 and H_2 . There are three different methods of activating the gaseous mixture: thermal (hot filament), electric discharge (microwave) or combustion flame (oxyacetylene torch).

All three methods have the same growth mechanism and share other similarities. For the purpose of this project hot filament chemical vapour deposition will be discussed. It is important to state one of the main disadvantages of hot filament is the fact that the filament will thermally degrade over time. This corrosion can lead to contamination. Additionally, the presence of O_2 in the chamber can result in filament destruction.

In the reactor the filament is made from either tungsten, tantalum or rhenium and is heated to temperatures of above 2400 K. A gas mixture of methane (CH_4) and Hydrogen (H_2), in the ratio 1:99 enters the chamber. If the concentration of methane is too high then it will result in the formation of graphitic carbon, as can be seen in the figure below. The gases pass over the substrate resulting in their activation.

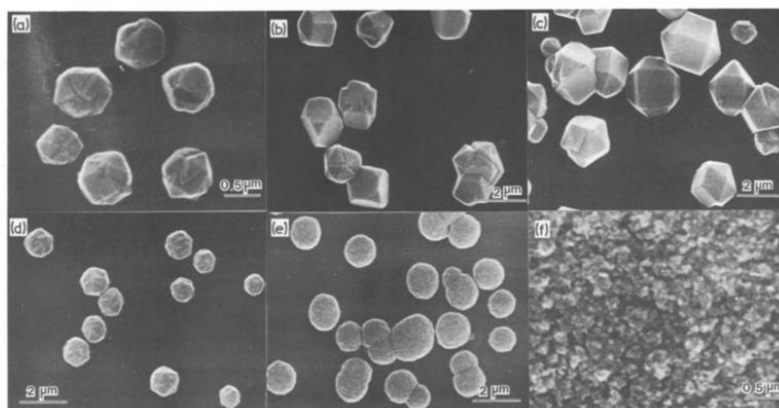


Figure 2: Effect of filament temperature on the deposits prepared at 1100 K under 37 Torr CH_4 (1%)- H_2 (a)-(c) and at 1150 K under 10 Torr CH_3 (3%)- H_2 (c), (d). Filament temperatures are (a) 2100 K C, (b) 2300 K (d) 2400 K (d) 2100 K (e), 2250 K (f) 2400 K. ¹⁷

Flow rate also plays an important role in diamond growth. High flow rates of $160 \text{ cm}^3 \text{ min}^{-1}$ can result in the formation of large ball like particles, which are co deposited with graphitic carbon. This is because higher flow rates result in faster carbon deposition which can exceed the rate of etching by H_2 ¹⁷.

Diamond crystallization by CVD works best at reduced pressures¹⁸. However if the pressure is too low then it means that only trace diamond particles with poorly defined habits can be observed.¹⁷ Therefore very specific pressure, temperature and flow rate conditions are needed. These can be seen in the table below.

Filament Temperature °C	Flow Rate / sccm	Pressure (Torr)
2500	H_2 (200)	8×10^{-3}
	CH_4 (2)	

Table 2: Typical conditions for diamond growth

4.4.3 Gas Phase Reactions

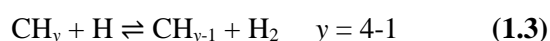
The activation of the gases results in fragmentation of methane and hydrogen into reactive radical species.



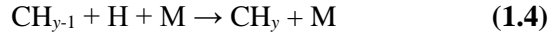
The recombination of the H radicals (1.1) is slow, and this therefore allows them to diffuse to the outer region of the reactor before recombining. This results in a concentration profile near the filament. This process allows them to reach the substrate before recombination can occur.

The hydrogen radicals can also react with the methyl radicals to reform methane (1.2). This recombination has a much faster rate than the formation of H_2 from H radicals. This therefore lowers the diffusion distance of the hydrogen gas, however the distance is still sufficient to allow for adsorption of hydrogen onto the substrate¹⁹.

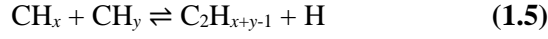
There are several other reactions that take place in the gas phase. One set of these reactions are known as H shifting reactions (1.3). Here the hydrogens of the hydrocarbon react with hydrogen atoms to produce H_2 gas and a variety of C_1 radicals.



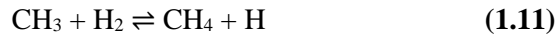
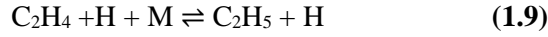
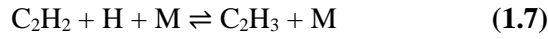
In cooler regions near the edge of the reactor the carbon can regain the lost hydrogen.



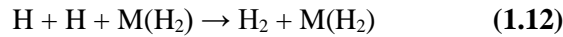
As filament temperature is increased there is a conversion from C_1 species to C_2 species (1.5, 1.6). This reaction is favoured where temperatures are between 1400 and 2200 K which can be found in the core of the plasma.



In the core of the plasma approximately 97% of the hydrocarbon species are C_2H_2 . The C_2 species can then undergo a series of H-shifting reactions (1.7 to 1.11) to regenerate the CH_3 radical used in diamond growth. These reactions are favoured in the outermost regions where $T_{\text{gas}} < 1400$ K.



The rate of H-shifting reactions increases with an increase in $[\text{CH}_4]$. It is also important to note that higher pressure in the chamber results in a decrease in H radicals (1.12).



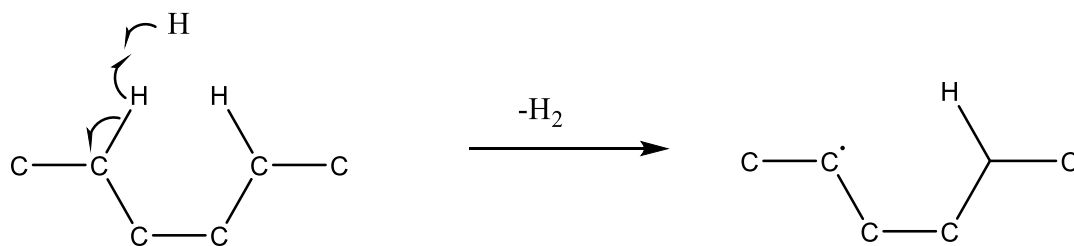
4.4.4 Diamond Growth

Deposition onto the diamond surface involves a series of adsorption/desorption processes. The larger the molecule the greater the entropic loss in regards to joining the carbon network. Therefore molecules with more than one carbon are less likely to attach themselves to the film. This means that the C_1 radical species are the most important in diamond growth. Papers have shown through isotopic labelling that 90% of the diamond originates from methyl radicals and the remainder from acetylene ($\text{H}-\text{C}\equiv\text{C}-\text{H}$)²⁰.

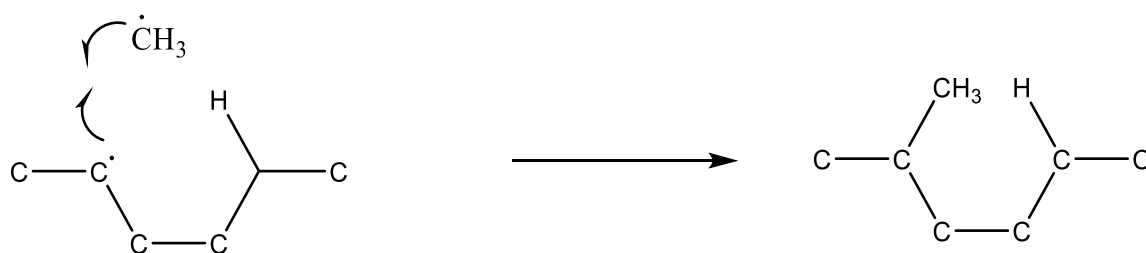
This agrees with thermodynamic data, since the attachment of the methyl radical has a ΔS value of -100 J K^{-1} . Acetylene has a slight more negative value which means its attachment is less favourable. This also means that even larger molecules which have a higher entropic loss or not likely to contribute to diamond growth^{21,22,23,24}.

The mechanism of how the diamond film grows can be seen in the diagram below. Initially the surface of the CVD diamond is almost entirely covered in hydrogen atoms (dangling bonds). This limits the number of sites that the CH_3 radical can adsorb onto the diamond surface. However, dangling bonds on

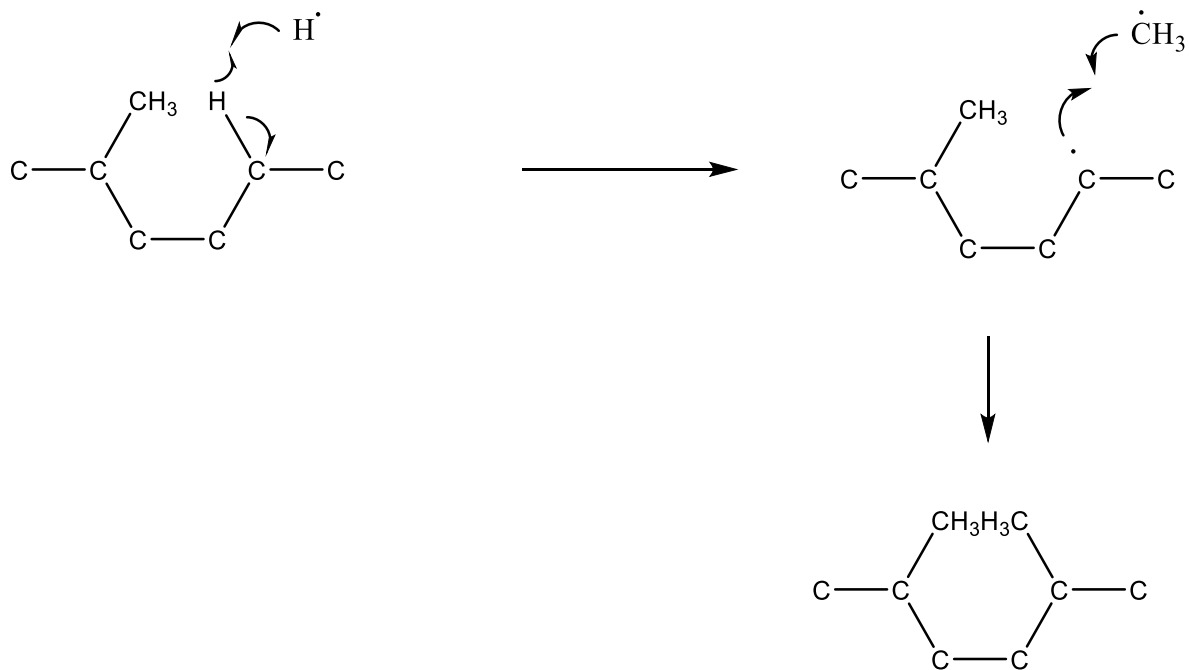
the surface of the diamond are far more reactive and therefore susceptible to attack from radicals. In the first step the hydrogen radical attacks the dangling bond, resulting in the formation of a carbon radical.



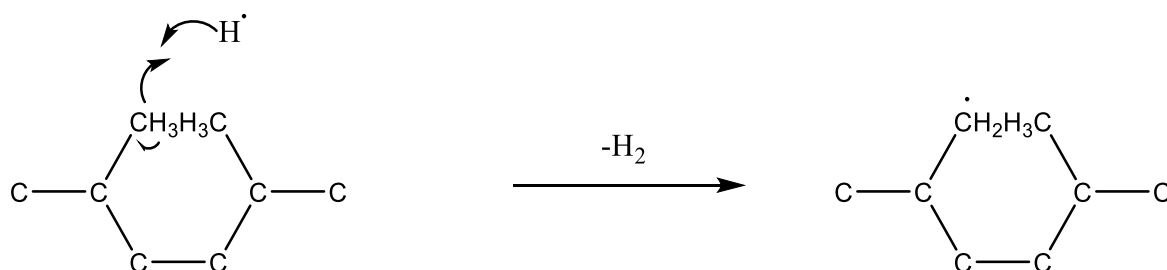
This can then undergo one of two reactions. One possibility is that a hydrogen can simply react with the carbon radical to give back the initial species. Or, a less likely outcome is that one of the CH_3 radicals present in the chamber can react with the carbon radical to form a new C-C bond. The re-attachment of hydrogen is favoured over the attachment of the methyl radical due to lower loss in entropy and greater $[\text{H}\cdot]$.



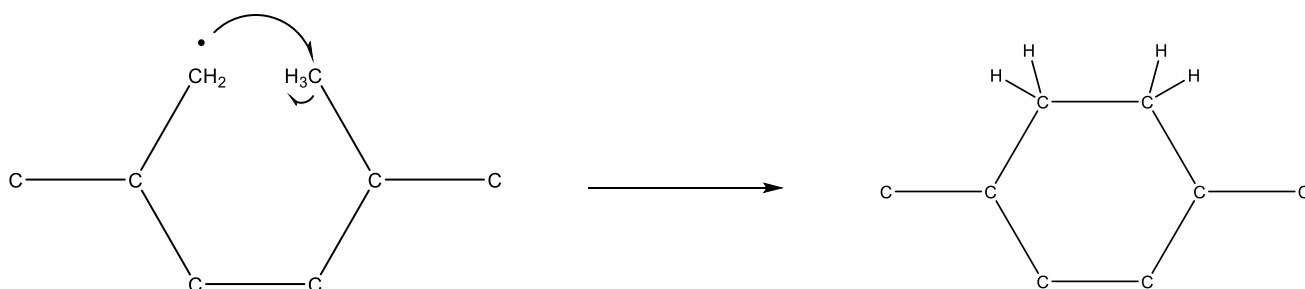
The attachment of the CH_3 radical leads to crystal growth. This process can be repeated on another carbon on the surface resulting in two hydrocarbons adjacent to one another.



The hydrogen radicals can now react with either of the hydrocarbons that have formed on the surface in another H abstraction reaction.



The final step in the growth process is the completion of the ring structure. Here the carbon radical attacks the adjacent hydrocarbon, resulting in the formation of a new C-C bond and the release of a hydrogen radical.



Growth of the diamond film is fastest in the direction perpendicular to the substrate. This forms a continuous film with a column structure, in a process known as evolutionary selection principle²⁵.

4.5 Doping

Doping is the introduction of impurities to an intrinsic semiconductor in order to change its electronic properties. As boron is of similar size to the carbon atoms its incorporation into the diamond lattice can be done with a small activation energy. This means that diamond with a high concentration of boron doped atoms can be achieved. As boron is to the left of carbon in the periodic table it results in p-type dopant properties. The doping results in deficiencies in valence electrons known as ‘holes’. Therefore holes, not electrons are the majority carrier in the semiconductor. This creates an acceptor level 0.37eV above the valence band maximum and thus makes diamond conducting²⁶.

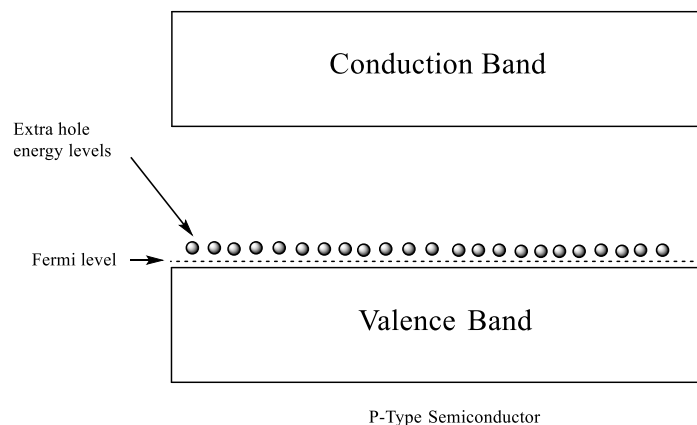


Figure 3: Diagram of the band gap in a p-type semiconductor

Boron doped diamond can be produced by incorporation of boron in the gaseous form (B_2H_6) into the CVD reaction chamber. This allows for the incorporation of boron into the diamond lattice. However too high of a boron doped concentration can affect the lattice and result in distortion.

Incorporation of nitrogen into the diamond lattice results in n-type semiconductor doping. Since nitrogen has one more valence electron than carbon it means that electrons are now the majority carrier. Additionally there are now electrons below the conduction band minimum. However this type of doping is harder to achieve in diamond as there is a high activation energy of 1.7 eV. Another downside to nitrogen doping is the fact that it is not conducting at room temperature. This is because the donor level is too deep into the band gap. Therefore thermal excitation is needed to generate electrical excitation.

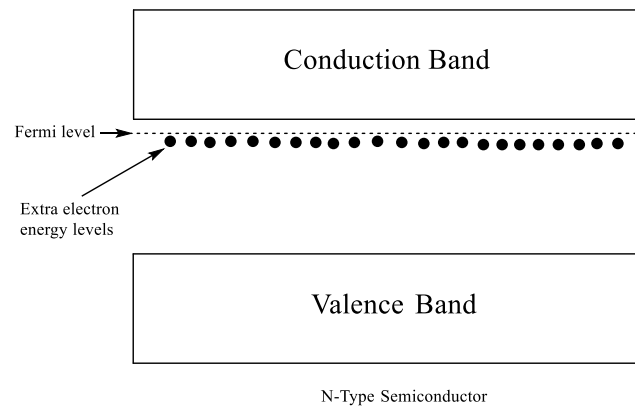


Figure 4: Diagram of the band gap in an n-type semiconductor

4.6 Diamond Surface

There are three different diamond faces that can be exposed, the (100), (110) and (111) faces. However, the two main surfaces are (100) and (111). The (110) surface which is present in natural diamond is rough under CVD and HPHT growth conditions²⁷.

Growth on these two surfaces depends on both temperature and gas composition. Growth of the (100) surface is greatest in a methane concentrations of 0.6% while growth of the (111) surface is greater in lower methane concentrations. As temperature increases the growth ratio of the (100) to the (111) surface increases. Additionally, it has been shown that both the (100) and (111) surfaces are grown by similar mechanisms, which result in only slight differences in the nanometre scale.

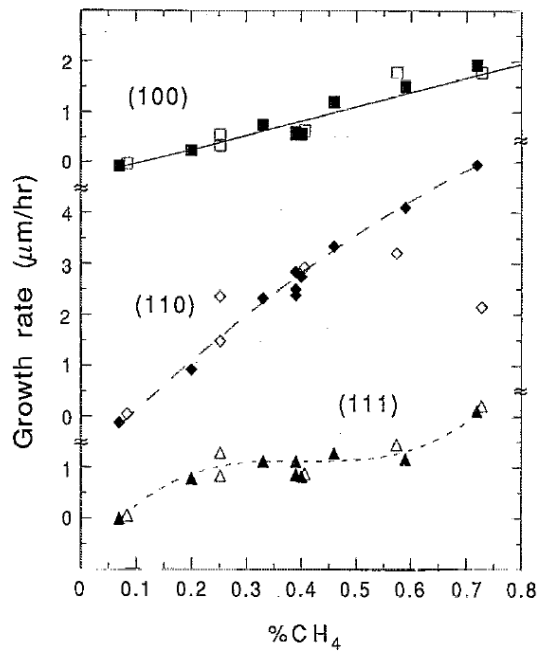


Figure 5: A line graph that shows the different growth rates of the CVD diamond surface in different methane concentrations²⁸

These surfaces can undergo surface reconstruction. This is where the atoms at the surface of the crystal rearrange to assume a different structure than the bulk of the crystal. Both the (100) and (111) surfaces show different reconstructions and behaviour when exposed to atomic hydrogen.

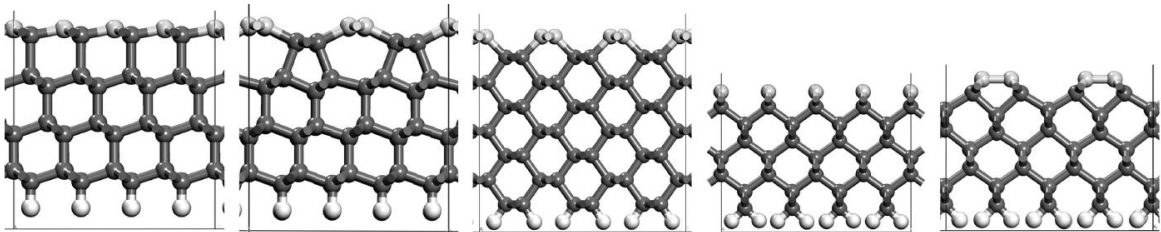


Figure 6: A side view of the models of diamond. The surfaces from right to left are: (111)- 1 x 1, (111) -2 x 1, (110) – 1 x 1, (100) 1 x 1 and (100) – 2 x 1²⁹.

4.6.1 (111) Surface

The (111) face has a cubic close packing arrangement and is therefore referred to as cubic. It can be cleaved by cutting one or three bonds per surface atom. The (111) face follows a stacking sequence of ABCABC which means that every third layer is identical. This also results in a higher impurity incorporation for the (111) plane.

The (111) plane is of significant interest since it can provide a surface for atomically smooth growth in CVD diamond. Here a hydrogen atom terminates each of the surface carbon atoms. Growth of the next layer on the cubic face requires the incorporation of three carbon atoms.

The hydrogen terminated (111) face has a simple unreconstructed structure up to temperatures of 1100 K. The (111) surface shows a 1×1 low energy electron diffraction (LEED) pattern. At greater temperatures the hydrogen present on the surface desorbs resulting in a 2×2 LEED. This is a result of the superposition of the three 2×1 rotational domains. This process is reversible upon exposure to hydrogen. The energy minimum on the surface is constructed from unbuckled π -bonded Pandey Chains. This is the reason why the electronic band structure of the (111) surface demonstrates no band gap^{30,31,32}.

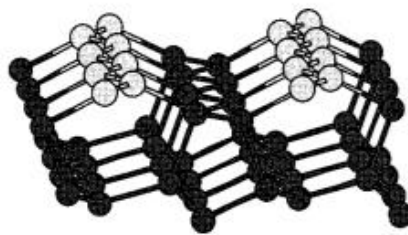


Figure 7: Pandey π bonded chain model of the (111) diamond surface

4.6.2 (100) Surface

The (100) face has a hexagonal close packing and is referred to as hexagonal. The cleave plane cuts two bonds per surface atom. For the (100) face the adjacent hydrogen bonds are closer in distance than those in H_2 . This causes the structure to alter itself sterically to satisfy the constraints. Therefore the fully H-terminated crystal will reconstruct in a 2×1 structure where two adjacent surface atoms move closer toward each other to form parallel rows of π bonded dimers. The dimers on the surface are symmetrically π bonded and unlike the Si (100) surface do not exhibit Jahn-Teller distortion. Deposition of the hydrogen monolayer on the surface increases the bond length of the dimer. Growth on the hexagonal face requires the incorporation of two carbon atoms³³.

At higher hydrogen coverage and higher chemical potential the (100) surface can reconstruct to a (3×1) phase. Unlike the (2×1) phase the (3×1) phase consists of alternating mono and di hydride units. This surface has been observed in the Si (100) surface but has only been proven to be stable by calculations. According to the calculation the bond lengths of the mono and di hydrides in the (3×1) reconstruction were similar to the ones in the (2×1) surface³⁴.

4.6.3 Surface Roughness

In CVD diamond the competitive growth of the diamond crystal can result in increased film roughness. This roughness can affect the surface termination resulting in lower coverage. There are several methods to improve surface roughness. One of the most common methods is through resin bonded wheel polishing. This technique can be used for both single crystal and polycrystalline diamond. This method can however result in substrate damage. Another mechanical method is via the use of Chemical Mechanical Polishing (CMP). CMP machines are used in conjunction with polyester polishing cloth and alkaline colloidal silica polishing fluid to polish diamond film³⁵.

One other common method is by implantation and lift off processes. This was reported by Thi et al. Here a sacrificial defective layer is created on the diamond surface by ion implantation. C⁺ or O⁺ ions are implanted on the surface in order to remove a thin layer of diamond film. Annealing then changes the damaged layer into graphite. Following this selective etching and lift off is used to remove the graphite layer. This results in a new smooth diamond surface³⁶.

HPHT diamond films tend to have smoother surface with less defects than their polycrystalline counterparts. One way of improving the HPHT surface through scribe polishing. This allows for the direction of the wear fracture plane to be confined. The diamond can be pressed onto a high speed rotating scribe which has diamond particles already embedded into it and can achieve a high surface finish of with $Ra < 1$ nm. This process also results in low damage to the surface.

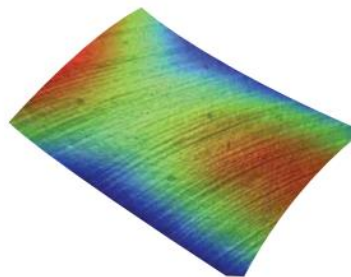


Figure 8: Surface produced by scribe polishing. The imaging was done through the use of atomic force microscopy. The grooves on the surface are < 5nm wide

The surface can be characterized by the use of several different techniques. Two of the most common are Scanning Electron Microscopy (SEM) and Atomic Force Microscopy (AFM). SEM allows for the determination of surface morphology and grain size, whilst AFM allows for the measure surface roughness³.

4.7 Surface Terminations

The dangling bonds on the diamond surface are hydrogen terminated following CVD synthesis. However through the use of wet or dry chemical methods these bonds can be changed to different elements. These new terminating species result in different surface properties (electron affinity, hydrophobicity and conductivity).

4.8 Hydrogen Terminated Diamond

4.8.1 Surface Structure

For the (100) hydrogen terminated diamond surface the mono-hydrogenated (2×1) surface is considered to be the most stable under normal conditions. This occurs when the monohydride structures form single bonded dimers³⁷.

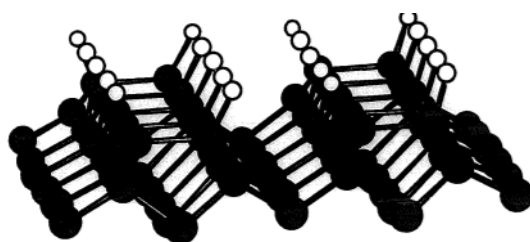


Figure 9: $2 \times 1:H$ structure of the (100) diamond surface. Here the structure is composed of monohydride dimers where each dangling bond is terminated by hydrogen³⁸

However, it is important to note that the hydrogen surface termination does not result in additional stabilization of the bulk diamond structure. The termination does however causes the π and π^* orbitals of the dimer to be replaced with the bonding and anti-bonding C-H orbitals. This causes the surface dimers to go from double to single bonded. This affects the surface states of the diamond and causes them to be shifted further in energy towards the conduction band. From Density Functional Theory (DFT) calculations we can see that the surface states are now 2 eV below the valence band maximum (VBM), whereas before it was approximately 5 eV above it.

4.8.2 Methods for Hydrogen Terminating Diamond

Hydrogen terminated diamond can be produced through the use of annealing in a H_2 environment, or through the generation of atomic hydrogen via plasma or hot filament reactors.

High temperature annealing at atmospheric pressure was first reported by Seshan et al³⁹. Here H_2 gas is flown into the reactor at a temperature of 850 °C. The surface properties were found to be similar to that of hydrogen plasma treated diamond films. The hydrogenation of the surface was a result of thermal

dissociation of surface functional groups which form active surface sites. These sites allow for the dissociation of the H₂ molecules resulting in C-H bonds forming on the diamond surface³⁹.

Unlike the annealing method both the hot filament and plasma reactor result in the dissociation of H₂ directly. The hydrogen species then go on to react with the surface of the diamond resulting in a hydrogen terminated layer. However the plasma termination can result in the etching of the diamond surface, whilst the hot filament reactor can cause surface contamination. This contamination is a result of deposition of filament material onto the surface⁴⁰.

It has also been found that exposure to hydrogen plasma can result in an increase in surface roughness. This is because the plasma can etch the diamond surface, which initially results in extended defects, such as dislocations, followed by anisotropic etching. This can be seen in the image below. AFM measurements revealed that 3 minutes of plasma exposure, at conditions of H₂ at a flow rate of 80 sccm/min at 30 torr at 850 °C, resulted in a surface roughness enhancement of 27 nm.

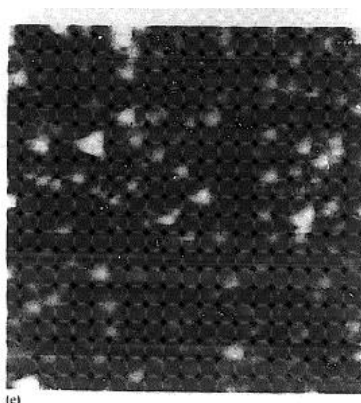


Figure 10: Increased surface roughness of type Ib HPHT diamonds due to exposure to hydrogen plasma⁴¹.

Hydrogen termination of boron-doped diamond can be achieved through the use of electrochemistry. By applying negative voltage in acidic solutions a clean hydrogen-terminated surface can be produced. This surface again exhibits similar properties to plasma treated H-terminated diamond. However the main drawback is that the diamond must be conducting (i.e. boron doped) at room temperature⁴².

4.8.3 Surface Conductivity

One of the features of hydrogen-terminated diamond is that it demonstrates surface conductivity when exposed to air. It shows p-type semiconductor properties. This means that holes are the majority carriers. However, in order for it to be effective as a semiconductor it needs layer of aqueous adsorbates in order to promote electron diffusion from the surface in order to create holes in the bulk.

The origin of the p-type conductivity is a result of several factors. One of these factors is valence band electron transfer into an adsorbate layer which results in surface band bending⁴³. Additionally H-termination causes hydrogen induced surface acceptors as well as deep level passivation by hydrogen, both of which result in p-type semiconductor properties⁴⁴.

Furthermore, the C-H bonds break the symmetry of the diamond which causes sub-bands to form. This lowers the band gap, as seen in figure 11, which makes diamond a semiconductor. However, there are several issues that need to be addressed. For instance, CVD diamond is a polycrystalline material and therefore contains grain boundaries, stacking faults and other defects, which reduce the lifetime of the semiconductor. Moreover, achieving further p-type doping through the incorporation of boron atoms has proven to be difficult. This is because the rigidity of the diamond lattice makes it difficult to incorporate other atoms into the system^{45,46}.

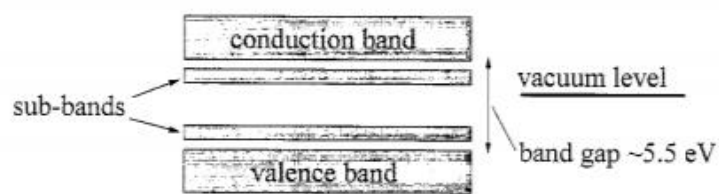


Figure 11: Band structure of diamond close to the surface. Here sub-bands are formed just below the conduction band just above the valence band⁴³

Hydrogen terminated diamond has been used as a semiconductor in both active (high-power switches) and passive devices (Schottky diodes). Diamond's remarkable thermal properties make it suitable for operation as a semiconductor material in high power, voltage, frequency or temperature environments⁴⁷.

4.8.4 Negative Electron Affinity and Secondary Electron Yields

Another of hydrogen-terminated diamond's main properties is its negative electron affinity (NEA). This can be determined by

$$NEA = \phi + (E_f - E_{VBM}) - E_{BG} \quad (2)$$

The terms in equation (2) are: ϕ is work function, E_f is the Fermi level, E_{BG} is the band gap and E_{VBM} is the valence band minimum.

For diamond, only the work function can be changed and the other three variables are all constants. Work function is defined as the minimum amount of energy required to remove an electron from the Fermi level to a point of infinite distance away from the surface. This change in work function is directly responsible for its negative electron affinity⁴⁸.

Since carbon is more electronegative than hydrogen there is a resulting movement of charge towards the carbon in the C-H bond. The electron density is then forced into the conduction band minimum which is above the vacuum level. This feature makes H-terminated diamond an interesting material for surface science.

If we change the terminating atom we can change the electron affinity. For example, termination with more electronegative atoms will result in electron density being drawn away from the conduction band.

Currently there are several potential applications for NEA diamond. Due to its: high, stable electron yield, wide band gap and thermal conductivity, diamond has several advantages over other NEA materials. One current project is the development of diamond materials as electron emission sources for thermionic energy generation. This is where solar energy is focused onto a diamond cold cathode, resulting in emission of electrons via thermal excitation of electrons. The electrons will then be collected at a nearby second electrode thus generating electricity^{45,49}.

The presence and extent of hydrogen termination on the diamond results in a rise in secondary electron yields. There are two main reasons for this. The first is the presence of a wide band gap which allows for low energy electrons to have large escape depths. The second reason is the low NEA at the surface which allow low energy secondary electrons that reach the surface to escape into vacuum⁵⁰.

4.8.5 Hydrophobicity

Hydrogen-terminated diamond is also hydrophobic in nature. The hydrophobicity arises from the C-H bonds on the surface which are poor H-donor and acceptors. Recently there has been an increase in demand for highly hydrophobic (HHP) materials. These are materials which the contact angle with water θ exceed 120° . These materials have become increasingly more popular in bio-medicine, energetics, electrochemistry and micro electrochemical systems⁵¹. Research by Ostrovskaya et al, have managed to create ultrananocrystalline diamond (UNCD) film with a contact angle of $106 \pm 1^\circ$. A contact angle of 124° was achieved by nanoporous hydrogenated diamond. This material was obtained by oxidation in air of nitrogen containing UNCD followed by treatment with a microwave hydrogen plasma⁵².

The contact angle measurement is based on Young's equation.

$$\cos(\theta) = \frac{\sigma_s - \sigma_{LS}}{\sigma_L} \quad (3)$$

The terms in equation (3) are: θ relates to contact angle, σ_s is surface energy of the solid, σ_{LS} is the interfacial energy between liquid and solid, and σ_L is the surface energy of water.

4.9 Oxygen Termination

4.9.1 Surface Structure

For the (100) (1×1) surface there are two plausible functional groups: the ether and the carbonyl. For the ether arrangement, the divalent oxygen atom bridges to two surface carbon atoms, while for the carbonyl arrangement the oxygen is double-bonded to one surface carbon atom. The axis of the carbonyl atom is normal to the surface. Hydroxyl groups can appear on the surface in the presence of atomic hydrogen⁵³.

Calculations on the (100) surface have shown the ether arrangement to be more stable than the ketone by 0.60 eV per oxygen atom. This is due to the fact that the highest occupied molecular orbital (HOMO) in the ether system is significantly lower than the ketone system.

For the (111) surface, partial uptake of oxygen occurs on the (2×1) surface at room temperature, without lifting the reconstruction. However, in order to achieve full monolayer coverage, temperatures need to be increased to 400 °C which then results in the (1×1) reconstruction of the surface. The same three groups that appear on the (100) surface, ether, ketone and hydroxyl, also appear on the (111) surface. Again hydroxyl groups only appear in the presence of atomic hydrogen⁵⁴.

Different oxygen-containing groups are produced by different oxidation techniques or exposures. Moreover, the nature of the oxidation also depends upon the diamond surface. Polycrystalline, nanocrystalline and single crystal diamond show slight differences following oxidation under the same conditions. This means that HPHT and CVD diamond behave differently with some methods.

Experiments showed that (111) CVD diamond was slightly more receptive than (100) diamond to oxygen plasma treatment. This was done by using XPS to quantify the amount of oxygen on both of the two surfaces.

The coverage for the (111) surface was 0.55 ML, opposed to a maximum of around 0.7 ML. Therefore, the surface was not fully terminated in diamond. For the (100) surface a coverage of 0.48 ML was achieved. The most prominent group that appears on both surfaces following oxygen plasma termination is the C-O-C ether⁵⁵. This was determined by analysing the chemical shift of the core C1s electrons through the use of XPS.

On the (100) surface as the coverage increases the percentage of carbon atoms in the second oxidation level (ketone, C^{+II}) increases, whilst the percentage of carbons in the carboxylic acid state (third oxidation level, C^{+III}) decreases.

On the (111) surface the opposite is observed. At long plasma exposures, the percentage of C^{+II} carbons is almost equal to those in the C^{+III} state. This can be explained by the fact that as you increase surface oxidation the Pandey chain of the clean surface is broken. Therefore at low termination percentages, the epoxy like C-O-C bonding will dominate. However at higher O coverage transitions to carbonyl and carboxylic acid species will occur as there will be a removal of the (2 × 1) reconstruction⁵⁴. However despite this increase in C^{+II} or C^{+III} in the different surfaces the ether group still remains the most prominent group.

4.9.2 Methods of Oxidizing Diamond

Oxygen termination can be achieved by four different techniques: electrochemical oxidation, thermal oxidation, wet chemical oxidation and oxygen plasma termination. Different methods deposit different groups on the diamond surface. It has been reported by Klauser et al, that plasma termination and wet chemical oxidation with sulfo-chromic acid at 230-250°C are the most successful and reliable methods of termination⁵⁵.

Other wet chemical methods include treatment with HNO₃/H₂SO₄ or H₂SO₄/H₂O₂. Wet chemical treatment with nitric and sulfuric acid will generate a large amount of acidic groups on the surface. The majority of these groups are carboxylic groups. However, tertiary and neopentyl alcohol groups as well as carbonyl groups with neighbouring hydrogens can contribute to acidity⁵⁶.

Ozone can also be used as powerful oxidizing agent for diamond termination. UV irradiation in an ozone environment resulted in an increased content of C=O groups on the diamond surface. Ozone oxidises the surface with two different reaction pathways. The first is partial dissociation of the ozone molecule which results in an alkoxide structure that is then converted to an epoxide like structure (figure 12). The other more prominent method of oxidation is by complete dissociation of the ozone molecule. This results in two of the oxygen atoms forming a ketone structure whilst the third oxygen forms the alkoxide structure which again is rapidly converted into the epoxide structure (figure 13)⁵⁷.

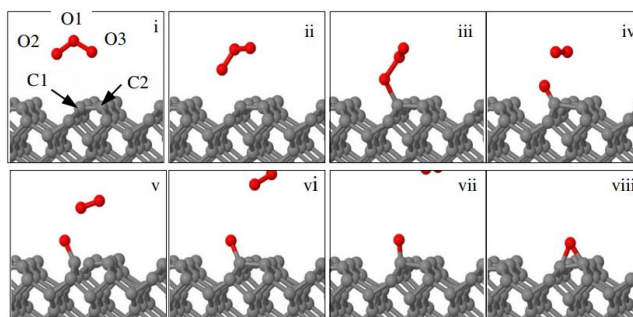


Figure 12: Partial dissociation of the ozone molecule on the diamond surface⁵⁷

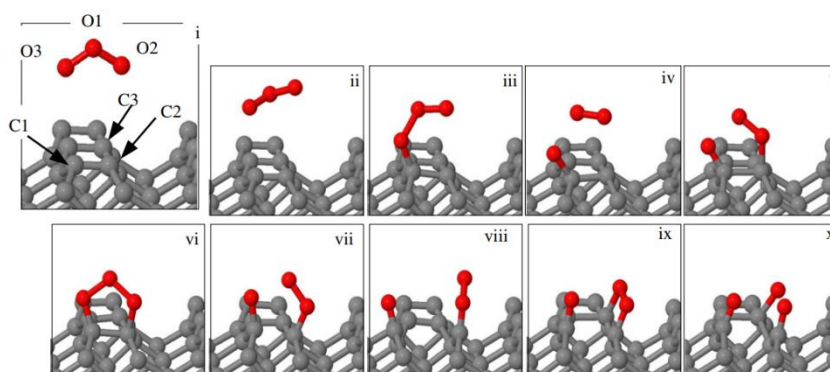


Figure 13: Complete dissociation of the ozone molecule on the diamond surface⁵⁷

Hydroxylation of the diamond surface can be achieved following oxygen termination. One method is with the use of borane or lithium aluminium hydride. These are both reducing agents which will convert the ketones present on the surface into hydroxyl groups. These hydroxyl groups can then be used to attach ligands to the diamond surface directly⁵⁸.

The presence of these hydroxyl groups can be confirmed through the use of silane reagents, since they are unreactive towards ether or carbonyl groups. One such example of this is the reaction with 3-aminopropyltriethoxysilane (APTES). The presence of silane groups was identified through XPS. This showed that hydroxyl groups must have been present on the surface for the APTES to react⁵⁹.

Thermal termination can also let you control the type of groups present on the diamond surface. At higher temperatures the oxidation state of carbon increases. This can be seen in the figure below.

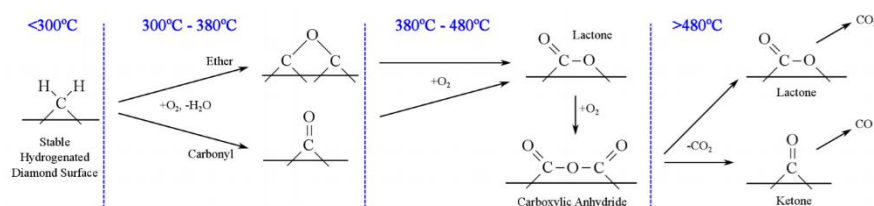


Figure 14: Oxidation reactions on a diamond surface at increasing temperatures. These reactions took place in an atmosphere of 20% O₂/Ar⁶⁰.

Moreover by first terminating the diamond surface in chlorine, Ando et al⁶¹, have shown that oxygen termination can take place at lower temperatures through the use of water present in the air. Additionally it allows for selectivity since at lower temperatures the hydroxyl group is preferred over the ketone. This acts as another way of producing hydroxyl groups.

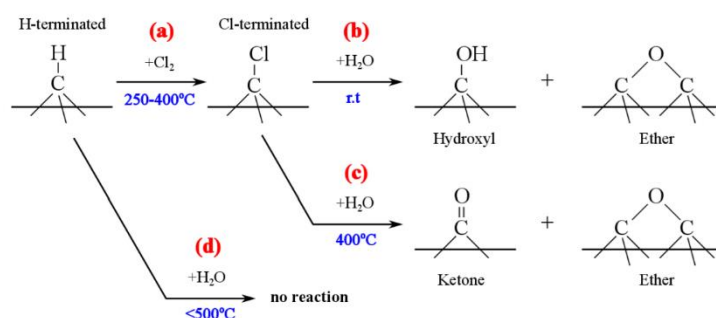


Figure 15: Reaction a takes place in 10% Cl₂/90% Ar₂ atmosphere. Between 500 and 700 K. Reaction b took place in air where water vapour reacted with the surface to produce the hydroxyl and ether groups. In reaction c diamond was heated while exposed to air resulting in the formation of the ketone group instead of the hydroxyl⁶¹.

4.9.3 Properties of O-Terminated Diamond

Oxygen termination results in a positive electron affinity (PEA) at the surface as well as a large ionization potential. This is because the more electronegative oxygen induces a δ^- charge on the surface layer, which acts to keep electrons within the surface. Kelvin probe force microscopy measurements (KFM) have shown that the Fermi level is about 0.7-2.0 eV above the VBM⁵³.

This results in PEAs of 2.6 eV for the ether configuration of the diamond surface. The meta-stable ketone configuration was found to have an even higher PEA of 3.6 eV. Hydroxyl termination will result in the surface having a NEA. This is due to the fact that the presence of the oxygen means that the CO dipole is now more δ^- than the carbon alone, which means the CO-H bond has a lower NEA than the hydrogen terminated surface⁶².

Following oxygen termination, the full recovery of the H-terminated surface is still not possible by heating in a H₂ atmosphere at low temperatures, as some oxygen species remain present on the surface. This is due to the fact that the oxygen present is converted into stable hydroxyl groups by the addition of atomic H at low temperature, high vacuum conditions. The hydroxyl species has no efficient escape route from the diamond surface at these conditions. However, by raising the temperature to 700 K full recovery becomes possible⁵⁴.

Oxygen termination has a significant effect on several properties including chemical reactivity and conductivity. Carboxylic acid groups on the diamond surface can be functionalized and thus used in chemical reactions. One such example of this is the reaction of oxygen-terminated diamond with 2,4-Dinitrophenylhydrazine (DNPH) which prevents the Fe^{2+/3+} redox reaction. DNPH covalently binds to the carbonyl group this increases the ΔE_p value which indicates a decrease in [Fe]^{2+/3+} redox reactions⁶³.

Oxygen termination also causes a depletion layer for holes. This is because of dense donor type surface states that exist 1.7 eV above the valence band. These surface states are responsible for band bending which is also responsible for high surface resistivity and thus electrical insulation.

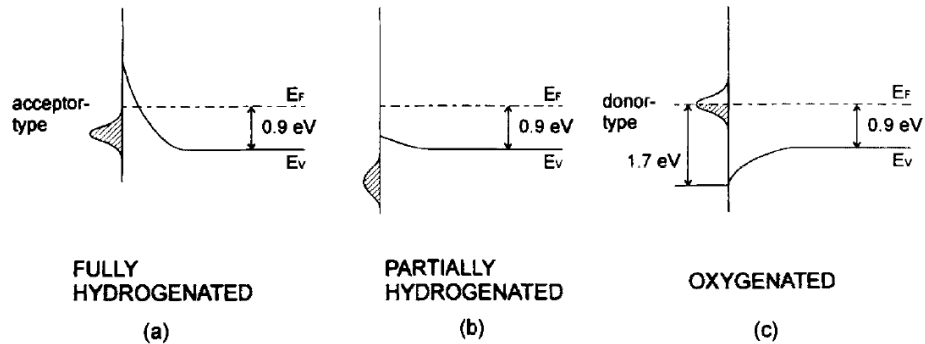


Figure 16: Energy band diagrams of full hydrogenated, partially hydrogenated and oxygenated diamond. Here we can see how oxygen termination causes surface band bending⁶⁴.

Oxygen termination also causes the diamond surface to become hydrophilic. This is because the direction and magnitude of the dipole is different to that of hydrogen. The oxygen-terminated diamond was found to have a contact angle of 47.2 °⁶⁵. The hydrophilic surface aids cell adhesion which in combination with diamonds bio compatibility has opened up research avenues in bio-electronics and tissue engineering⁶⁶.

4.10 Fluorine Terminated Diamond

4.10.1 F-Terminated Surface

The (111) and (100) diamond surface show different properties when it comes to fluorine termination. 75% F coverage was achieved on the (111) surface while only 50% was achieved on the (100) surface. This is due to greater steric hindrance of the C-F bond on the (100) surface. The addition of two fluorine atoms per surface carbon atom results in an F-F separation that is less than that in molecular fluorine. Work by Pederson and Pickett showed that the (100) surface therefore undergoes some reconstruction to accommodate the fluorine atoms. This leads to a disordered surface with regions of (1 × 1) and (2 × 1) reconstruction, as well as areas of non-fluorinated carbon with dangling bonds⁶⁷.

Additionally uptake of the F atoms varies depending upon the surface. On the (100) surface, uptake of the F atoms follows 2nd order kinetics. This implies that neighbouring reactive sites are affected by the uptake of fluorine on the surface. On the (111) surface uptake is 1st order and depends on fractional fluorine coverage. There are two different views on the surface structure of the fluorine absorption on the (111) surface. Freedman et al. have reported that F atoms break the π -bonded Pandey chains to form

regions of bulk 1×1 reconstruction. Upon annealing and desorption of the fluorine terminated species, the diamond surface reverts back to a 2×1 reconstruction⁶⁸.

An alternative view was proposed by Yamanda et al. who, based on LEED patterns, believe that the fluorine atoms interact with the Pandey Chains without breaking them. However, since fluorine atoms in organic systems will attack carbon-carbon bonded π orbitals in order to form bonds with the carbon atom, this theory is less likely. Furthermore, they speculate that the F atoms can penetrate into cavities between the top two rows of the diamond surface. However, this too, has proven to be unlikely as it would require large amounts of energy to distort the lattice in order to allow for the F atoms to penetrate.

Desorption of the F atoms occurs at a range of temperatures between 500 and 1200 K. This was measured by looking at the change in the F1s peak in the XPS spectra. For both the (100) and the (111) state the coverage decreases steadily as temperatures rise until all the fluorine is removed at approximately 1100-1200 K. This implies that there are a range of binding sites on the surface with a corresponding range of energies.

The (100) surface also exhibits two separate desorption regimes, whilst the (111) surface only exhibits one. Like hydrogen, the fluorine atoms will break surface dimers and thus desorb without etching diamond⁶⁸.

4.10.2 Methods for Fluorinating the Diamond Surface

The diamond surface is unreactive to molecular fluorine (F_2). Therefore, reaction conditions that generate atomic fluorine are needed. F_2 can only be used to terminate diamond in extreme and corrosive conditions. One such example is the use of F_2 gas at 470 °C⁶⁸. Milder conditions can be used to achieve fluorine termination with the use of photochemical reactions. Nakamura et al. fluorinated H-terminated diamond surfaces with the use of perfluoroazooctane. Perfluoroazooctane dissociates to give two perfluorooctyl radicals, which then abstract an H from the surface. Another perfluorooctyl radical can then react with the surface carbon radical to yield fluorine-terminated diamond⁶⁹.

One of the most common and successful methods for fluorine termination is through the use of a plasma reactor. A variety of gases can be used to form the plasma, however they must all result in the formation of fluorine species which will then result in the termination of the surface. Some of the most common gases include: SF_6 , XeF_2 and CF_4 .

4.10.3 Properties and Uses of Fluorine-Terminated Diamond

The C-F bond is the strongest single bond in organic chemistry, and in the case of diamond, stable up to temperatures of 1000 K. This makes the incorporation of it into organic molecules very useful. Fluorine-terminated surfaces are hydrophobic, despite the C-F bond being polar. Thus these bonds

exhibit ‘polar hydrophobicity’. This is due to the fact that the C-F bond is considered to be a weak hydrogen-bond acceptor, even with regards to the C-H bond. The fully fluorinated surface has a maximum adsorption energy of 0.09 eV, whereas the fully hydrogenated surface has one of 0.07 eV. However, a jointly fluorinated and hydrogenated surface results in both the HOH-HC and HOH-FC bond lengths decreasing. Therefore, this means that a decrease in F or H content causes the other hydrogen acceptor and donor abilities to increase^{70,71}.

Moreover, recent research has shown that fluorine and oxygen terminated surfaces result in higher and more stable negatively charged nitrogen vacancies (NV⁻). A negatively charged nitrogen vacancy is a point defect that occurs in diamond. Since both fluorine and oxygen terminated diamond have a PEA this results in a high density of NV⁻. Electron spins at these centres can be manipulated to give photoluminescence. Therefore, coupling external spins to the NV⁻ increases photoluminescence. Neutral charge state defects can also exist (NV⁰), however these do not exhibit the same optical and spin properties.

Due to the more electronegative fluorine atom, the electron affinity of the F-terminated surface is 0.43 eV higher than that of the oxygen-terminated surface. This makes it a better candidate than other terminated diamond surfaces for biotagging, magnetometry and quantum information processing^{72,73}.

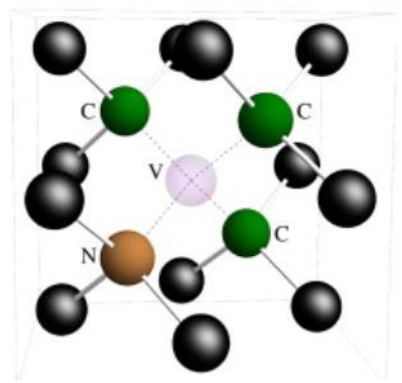


Figure 17: Nitrogen vacancy centre in the diamond lattice⁷⁴.

Fluorine-terminated diamond also shows a lot of potential as an electrode in aqueous solution. It displays the widest range of potentials (5 V) of any of the terminated diamond surfaces. One group has managed to use a boron-doped fluorine-terminated diamond as a pH insensitive Solution-Gate-Field-Effect Transistor. They achieved a sensing sensitivity of 27 mV/pH in a pH range of 2-10⁷⁵.

4.11 Nitrogen/Ammonia termination

4.11.1 Nitrogen-terminated diamond surface

Nitrogen termination results in the formation of a stable surface. There are essentially no sub-bands present in the surface states. Moreover, like oxygen and fluorine terminated diamond it has a positive electron affinity. Calculations have found the value for the PEA to be 3.32 eV. These features result in near-surface nitrogen vacancy centres which, as stated previously, can be used in magnetic and quantum sensing⁷⁶.

Nitrogen substitutes the carbon atom in the top layer of the 2×1 reconstructed (100) surface. This means that the surface does not undergo reconstruction from H to N-termination. However, the substitution of nitrogen causes the 2×1 reconstruction to stiffen in the (100) surface, whilst for the (111) surface the distortion and stiffening of the surface is less pronounced and exhibits an enthalpy of formation 0.3 eV/atom lower than that of the (100) surface.

Ammonia plasma treatments affect the surface slightly differently than nitrogen termination. Research has shown that the (100) and (111) surface of diamond both respond differently to the termination reaction. The (111) surface is terminated with the NH_2 group whereas the (100) surface will change to imine groups. These imine groups may then go on to form secondary amines, C-N-C.

The ammonia-terminated diamond surface should be kept under inert conditions. This is because the surface can react with water in the air, which then replaces the $-\text{NH}_2$ groups with $-\text{OH}$ groups. This was shown by the use of XPS and contact angle measurements. One of the suggested mechanisms for this process is by the protonation of the ammonia groups resulting in ammonium ions (R-NH_3^+). The ammonium is a good leaving group and undergoes a $\text{S}_{\text{N}}1$ reaction with hydroxyl groups.

4.11.2 Methods for achieving nitrogen/ammonia terminated diamond

Since the C-N bond is very stable, the introduction of the nitrogen atom can be done quite easily. One of the most interesting nitrogen containing compounds however is ammonia, as it can then go on to form amide bonds. Incorporation of these groups has normally been done by dry methods. The first reported case was in 1996 when chlorinated diamond was reacted with ammonia gas. Since then there have been many other dry methods which include the chemical treatment of the chlorinated surface, UV irradiation in ammonia gas and use of radiofrequency plasmas of He and NH_3 mixtures. However in some cases this has resulted in an increase in sp^2 carbon on the surface.

Moreover, there have also been some functionalizations performed in wet chemical conditions. A NH_3 solution containing persulfate as an oxidizer was able to successfully produce an NH_3 -terminated diamond surface. Another wet chemical method is the use of cysteamine. Cysteamine was added to

acid-chloride-terminated nanodiamond in toluene. The solution was kept at pH 10 and stirred at 80 °C for 12 h⁷⁷.

Nitrogen termination on its own can be accomplished through the use of a N₂ plasma. The plasma results in dissociation of the nitrogen molecule into separate atoms which can then go on to react with the diamond surface. Extreme plasma conditions are needed due to the strength of the N₂ triple bond. A 36 W, 40 kHz radio frequency (RF) generator with a N₂ gas flow rate of 11 sccm was used to successfully carry out a nitrogen termination⁷⁸.

4.11.3 Applications of Ammonia Terminated Diamond

Ammonia termination allows for subsequent chemical tethering via amide linkages. One such example of this is the attachment of horseradish peroxidase enzyme onto the surface. This was done by reacting the carboxylic acid group on the enzyme with the ammonia group present on the diamond surface. The reaction was carried out by placing the aminated diamond surface in a solution of the enzyme with a phosphate buffered saline (pH 7.4) for 24 h.

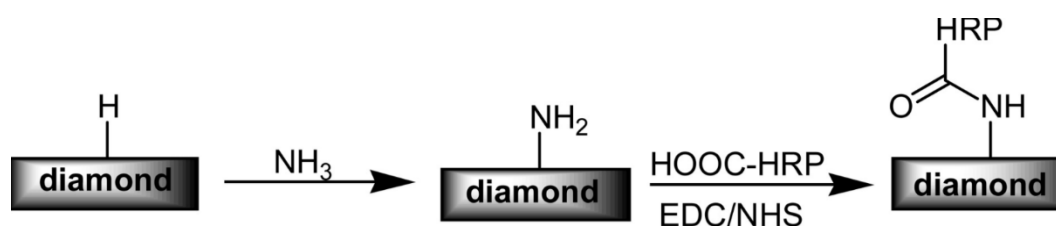


Figure 18: Attachment of Horseradish Enzyme onto diamond surface⁷⁹

An amine's high nucleophilic nature also makes it ideal for coupling reactions. These reactions can take place in aqueous media and result in the direct attachment of biologically important molecules, like proteins, to semiconducting CVD diamond.

Yang et al., have conducted coupling reactions by reacting one of the amine groups with 10 amino-dec-1-ene molecules protected by a trifluoroacetic acid group (TFAAD). 4 μL of TFAAD was homogeneously distributed on the diamond surface and then nitrogen purged in UV light illumination^{80,81}.

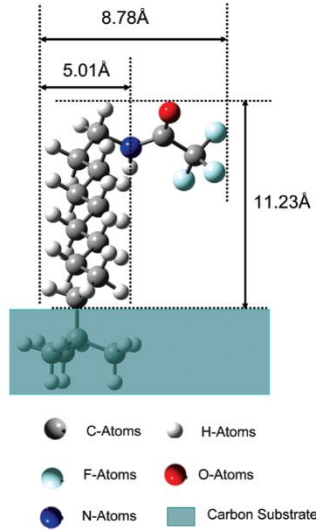


Figure 19: Illustration of TFAAD attached to diamond using a ball and stick model. Chain length was determined by Gaussian98 using B3LYP calculations⁸².

4.12 Plasma Termination

As plasmas can be used to perform all the prior discussed termination reactions, it is important to discuss how plasmas are generated. Plasmas can be formed artificially, however in order to form the plasma strict parameters and characteristics must be met regarding ion species purity, uniformity and service lifetime. There are several different discharge methods for plasma formation such as microwave, arc or glow.

The amount of voltage needed to form a self-sustaining electric arc plasma is given by Paschen's Law (4). The voltage must exceed the breakdown voltage (V_B).

$$V_B = \frac{Bpd}{\ln(Apd) - \ln\left[\ln\left(1 + \frac{1}{\gamma_{se}}\right)\right]} \quad (4)$$

Here A and B are both constants that are experimentally determined. They can be assumed to be constant for a restricted E/p range. However this range depends on the gas composition. Here, p , acts as pressure and, d , refers to the distance between the two electrodes. Once there is a sufficiently large electric field present then ionization of the molecules occurs.

It is important to note that V_B increases with distance between the two electrons. This can be seen in the equation below.

$$p_0 d = \frac{V_B}{\left(\frac{E}{p_0}\right)} \quad (5)$$

Breakdown voltage is dependent on the product of gas concentration, p_0 , and the distance of the two electrodes, d . E_0/p_0 corresponds to the process associated with the movement of electrons in the glow discharge. Here E relates to the electric field strength and p_0 the pressure at 0 °C.

Some gases do not ionize well in plasmas and therefore mixtures can lead to better plasma density. For example a mixture of 50:50 O₂/Ar increases the plasma density. This is because Ar can help dissociate the O₂ which results in an increased O-atom density despite dilution of the feed gas⁸³.

4.13 Alternative Functionalization Methods

4.13.1 Surface Functionalization

There have also been recent developments in the field of surface functionalization. This is defined as the introduction of functional groups in order to aid electro catalysis or chemical reactivity⁸⁴. This can be done on CVD diamond and doesn't require specific termination reactions.

One such example is done via the introduction of a thiol group (SH) onto the diamond surface. This enhances the electrocatalytic properties of diamond. Moreover, the thiol can be expected to improve the electron transfer kinetics of the diamond surface. The thiols were attached to the molecule by first photochemically inserting an alkene bond into the C-H of the diamond. This was explained by Hamers et al.⁸⁵, who showed that UV light generates a photoelectron from the diamond valence band. This is then promoted to the π^* LUMO of the terminal alkene. The alkene can now insert into the hydrogen-terminated surface of the diamond, thus producing a carbon-carbon bond.

The other end of the alkene chain is a protected amine group. The protection group, tert-Butyloxycarbonyl (BOC), was then removed, this was followed by amine alkylation⁸⁶. The thiol was then added by radical addition of thiol acetic acid. This process is demonstrated in the figure shown below.

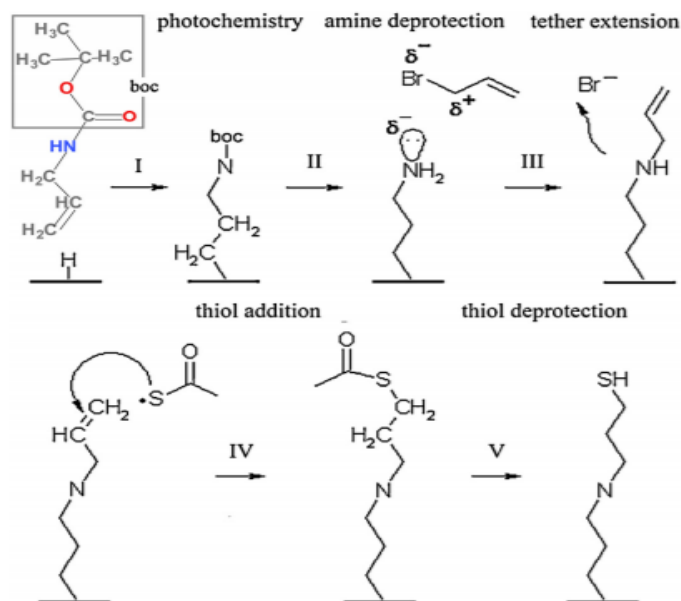


Figure 20: Thiol functionalization steps⁸⁶.

Another example is by the electrochemical reduction of aryldiazonium salts. The dinitrogen group attached to the benzene ring acts as a very good leaving group, which alongside its electron-withdrawing nature make it easy to reduce. The mechanism of the reduction and attachment of the salt can be shown below.

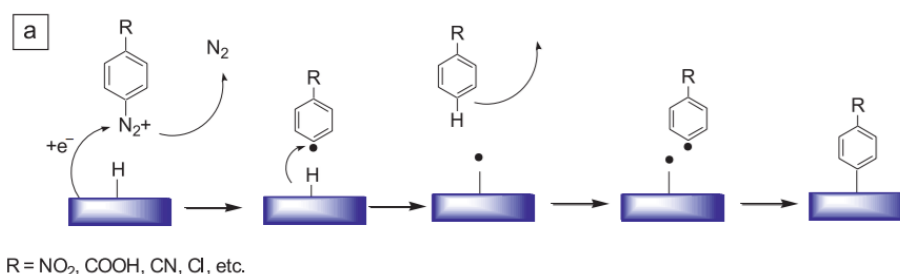


Figure 21: Reduction of aryldiazonium salt and attachment of benzene ring onto the diamond surface.

In the diagram above, the reduction of aryl diazonium salt to the radical was reported to have occurred on boron-doped diamond at -0.17 V. The R group present on the aryl ring can vary in nature and this can lead to different properties of the functionalized surface. For example, a nitro group can be reduced to an amine which can then be used to link biomolecules of interest. One downside of this method is the difficulty of forming a monolayer on the surface, since the phenyl radical species can also react with the already grafted phenyl rings.

4.13.2 Photolithography

Photolithography has allowed for the micropatterning of the diamond surface. This has resulted in multi-terminated layers with both hydrophobic and hydrophilic regions. These different regions show identical surface roughness and consist of fluorine, hydrogen and oxygen terminated areas.

Fluorine-terminated diamond is used as the starting point in producing diamond with both hydrophobic and hydrophilic areas. The diamond is covered in an image reversal photoresist with a thickness of roughly 1 μm . The surface is then exposed to a pure oxygen plasma⁵². Regions with the photoresist protect the fluorine termination whilst the other regions become oxygen terminated. Acetone is then used to remove the photoresist. This technique allows for the realization of multi-terminated surfaces in any desired size or geometry. Hydrogen-terminated regions were a result of the initial sample not being fully fluorine terminated prior to application of the photoresist.

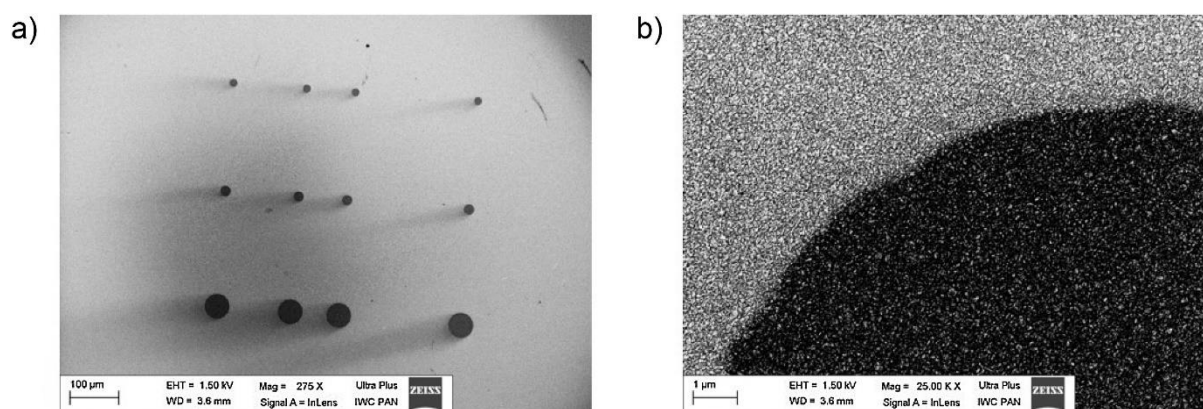


Figure 22: SEM image of fluorine-terminated diamond with varying diameter in a surrounding oxygen terminated surface. The difference in surface conductivity allows for the visible difference.⁵²

The fluorine and oxygen on the surface was confirmed through the use of X-ray Photoelectron Spectroscopy (XPS) and Energy Dispersive X-ray spectroscopy (EDX). Lateral force microscopy showed that friction in the hydrophilic region (oxygen terminated) was lower than in the hydrophobic region (fluorine terminated), despite the roughness being the same.

This material has several potential applications ranging from MEMS coatings, microfluidic biosensors and even solar energy harvesting⁸⁷. Additionally, having regions of different hydrophobicity with similar roughness will provide good receptivity for microbiological studies. Moreover, using similar techniques different multi-terminated regions can be realized.

5. Material Preparation and Experimental Techniques

5.1 Project Aim

The aim of the project is to modify an oxygen plasma reactor already present in the Bristol University Diamond Lab so that it can create F and NH₃ terminated diamond surfaces. Following the construction, HPHT diamond samples would undergo fluorine, ammonia and oxygen terminations. The resulting surfaces would then be characterized through the use of contact angle measurements, XPS and SEM in order to determine if the terminations had been successful.

5.2 Sample Preparation

5.2.1 HPHT Diamonds

For this experiment square HPHT diamonds supplied from Element Six's 4 point catalogue were used to perform the termination reactions. As supplied, the diamonds were polished on one side with the use of a scaife. The polished side has a surface roughness of < 30 nm and a (100) face. The edges of the diamond were laser cut and also have (100) edges. The length of the pieces were 2.6 mm with a thickness of 0.5 mm.

The diamonds are type Ib which means that they contain single substitutional nitrogen. The nitrogen-doped concentration of the diamond samples are < 200 ppm, with a boron doped concentration of < 0.1 ppm.

These types of diamonds were selected due to their smooth surface which would be more susceptible to plasma terminations. Additionally, all of the pieces are essentially identical which would improve the accuracy and reproducibility of the results.

5.2.2 Acid Clean

All of the HPHT samples were refluxed in H₂SO₄ (30 M, 100 ml) at a temperature of 280 °C for 6 h. They were then left to cool to room temperature. Following this, they were decanted and washed with deionized water. This was done until the samples were neutral in pH. The samples were then left to dry overnight. The purpose of the acid clean was to remove trace element impurities from the diamond surface.

Acid cleans using sulfuric acid have been found to oxygen terminate the surface. The exact nature of these groups vary depending on the conditions, however carboxylic acids, ketones and ethers are the most prominent groups on the surface.

5.2.3 Boron Doping

Boron doping of the diamond samples were performed so that they would be conducting. A conducting diamond surface was needed for NanoESCA analysis. A thin B-doped layer was deposited onto the HPHT substrates using the HFCVD reactor present in the University of Bristol Diamond Lab. A schematic diagram of the machine can be seen below.

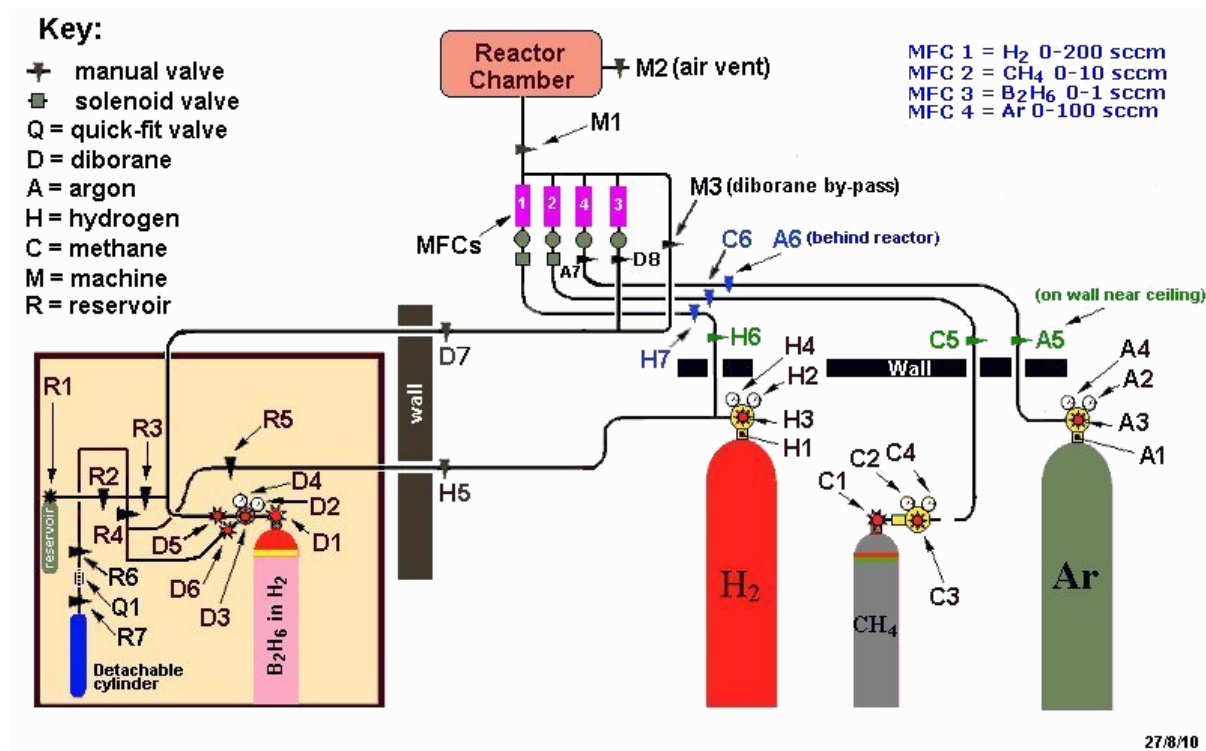


Figure 23: Schematic diagram of the HF reaction chamber used to Boron dope the diamond samples.

The reactor consists of: a reaction chamber, gas feed and a process gas removal. The reaction chamber was made of stainless steel. Samples were placed on a Mo holder that was resistively heated from below using a DC bench power supply (HQ-Power, PS3010). The diamond samples were also heated using the filaments which were made from tantalum. The filament wire had a diameter of 0.25 mm and was located approximately 3 mm above the diamond sample. Current was supplied to the 3 filaments using a digimess SM3040.

Pressure in the chamber was measured by two separate gauges: a capacitance manometer (Vacuum General, CMLB-21) and a Pirani (Edwards, PG100-XM). Gases were brought into the system using stainless steel piping and removed using a rotary pump (Leybold Trivac D8B).

A boron-doped hydrogen-terminated layer of diamond was deposited on the polished side of the diamond surface. A gas composition of H₂ (200 sccm), 5% B₂H₆ in H₂ (0.1 sccm) and CH₄ (2 sccm) flowed through the reaction chamber at a constant pressure of 20 Torr, controlled by independent mass

flow controllers. The filaments were heated by passing a current of 25 A through them. This caused their temperature to increase to 2000 °C whilst the temperature of the diamond sample was approximately 850 °C. The reactor ran for 1 h which resulted in a boron-doped film thickness of 1-2 μm.

For CVD diamond, this can increase the quality of the crystals at the interface as it can remove graphitic material and reduce grain boundary size. However for HPHT diamond this can affect surface roughness which means that the surfaces may now longer not be identical. This can affect future results like contact angle measurements.

5.2.4 Hydrogen Termination

Prior to exposure to the SF₆ or NH₃ plasma, the samples were hydrogen terminated. This was done using a microwave CVD reactor, and was performed in order to ensure that all the samples had identical starting terminations. The MW reactor can be seen in the image below. Gases were brought into the reaction chamber through the use of stainless steel pipes. The reaction chamber itself was also made from stainless steel and is water cooled. On top of the chamber was the magnetron (1.5 kW, 2.45 Ghz, Seki-ASTeX microwave generator). In the chamber the heated gas was excited to form a plasma ball through microwaves that create a resonant electromagnetic field pattern. The diamond samples were approximately 1 mm below the generated plasma ball.

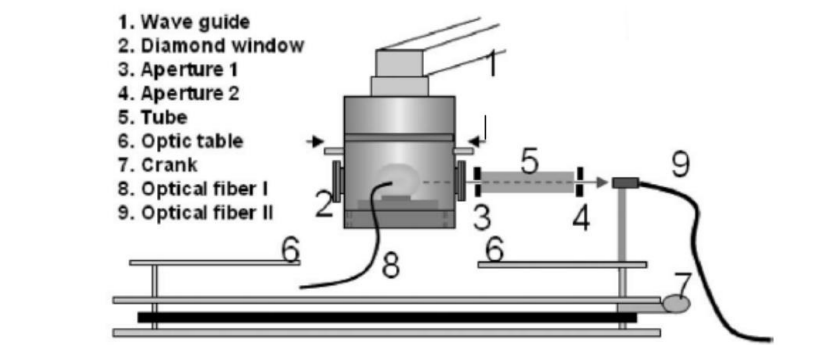


Figure 24: Schematic diagram of the microwave CVD reactor⁸⁸

A base pressure of 1.5×10^{-3} torr was established in the reactor prior to the introduction of hydrogen at a pressure of 110 torr. A plasma was generated for 2 mins at 110 torr of pressure and substrate temperature of 800°C using a power of 1250 W. Following this, the pressure of hydrogen was reduced to 45 torr and the temperature to 500°C with a power of 760 W. The conditions were kept constant for 2 mins before reducing the power to 0 W at a pressure of 45 torr. Following this the samples were allowed to cool down to room temperature prior to removal.

Hydrogen terminations were performed as a way of removing any impurities present on the surface of the diamond. Furthermore, it acts as a way of removing the oxygen termination from the acid clean. By fully hydrogen terminating the surface each sample that would go into the plasma reactor would in theory be identical (2×1 H-terminated), allowing for more accurate results. Additionally, hydrogen is less stable than both the nitrogen and fluorine terminated surface. Therefore, by having a hydrogen terminated surface subsequent terminations would become easier to perform.

5.3 The DC Plasma Termination Reactor

5.3.1 Construction of a Plasma Termination Reactor

The original reactor was a sputter coater (Edwards, S150A) that was modified into an O₂ plasma reactor. Sputter coating occurs when there is erosion of a target material by bombardment of heavy particles, in the presence of gaseous glow discharge between an anode and cathode. By feeding oxygen into the reaction chamber the sputter coater was modified to allow for the generation of an oxygen plasma and thus O-termination of the diamond surface.

The reactor consists of 5 main parts:

1. Gas feed
2. Process gas removal
3. Cabinet assembly
4. Vacuum chamber
5. Sputter head.

The gas feed and process gas removal were both parts of the modification made to the original sputter coater. The gas feed was made up of stainless steel pipes that bring oxygen and argon into the reactor. The flow rate was controlled by two N₂ mass flow controllers (MFCs). The process gas removal was done by a rotary pump (Leybold Trivac D10E).

The cabinet assembly was used to support the vacuum chamber. It also contained the power supply, a semi-rectified AC source which was capable of achieving a voltage of 2.1 kV. In the cabinet there were separate gauges for reading pressure. A Pirani Edwards APG100 was used to measure pressure up to 0.1 mTorr and a capacitance manometer (Baratron) used to measure pressures of 0.1 Torr and higher.

The vacuum chamber consisted of a stainless steel anode and cathode. It also contained a borosilicate plasma shield, which prevents the spread of the plasma. Furthermore, the presence of a more conducting copper plate (and the earthed pedestal supporting it) meant that the circuit is only complete when gas

flows through the chamber. Moreover, neodymium magnets increase plasma stability through the magneto caloric effect. The sputter head sat on top of the vacuum chamber however this does not have any role in surface termination. A rubber O ring is used to help achieve an airtight seal in the reaction chamber. The schematic diagram below is of the reactor prior to any modification.

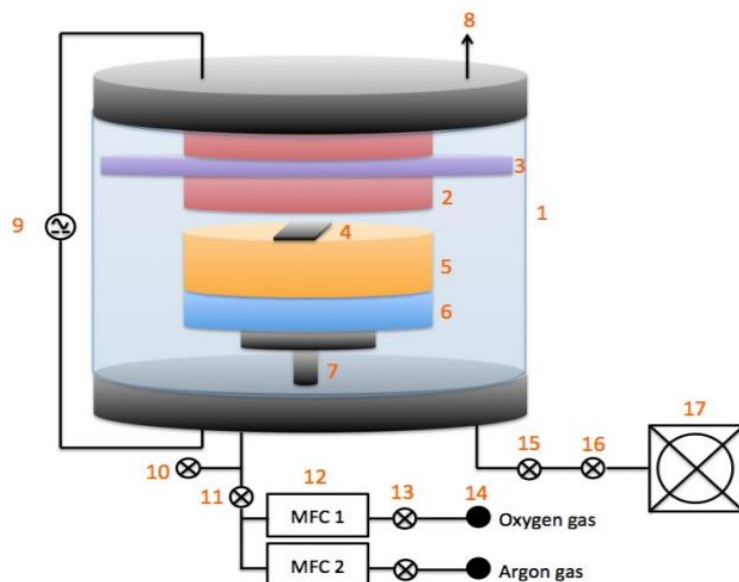


Figure 25: Schematic diagram of the O-termination plasma reactor. The labelled components are as follows: 1- vacuum chamber; 2 – cathode; 3 - plasma shield; 4- diamond sample; 5 – anode; 6 – conducting copper plate; 7 – grounded pedestal; 8 – line to gas inlet; 9 – power source; 10 – vent to air; 11 – gas inlet; 12 – MFC for both Ar and O; 13 – valves for the Ar and O lines; 14 – gas cylinders; 15 – needle valve; 16 – shut off valve; 17 – Leybold Trivac rotary pump⁸⁹

During the construction of the reactor, the gas feed was modified to allow for SF₆ and NH₃ to flow into the reaction chamber. SF₆ gas was used for fluorine termination whilst NH₃ gas was chosen for ammonia termination. One extra stainless steel pipe was added to the manifold which would bring either NH₃ or SF₆ into the system. Only one pipe was added since there would not be a need to use both of the gases at the same time. The pipe was also designed so that the mass flow controllers could be easily removed from the line, this makes the switching of the two gases less troublesome. A new readout box was added for the NH₃ and SF₆ mass flow controllers.

Furthermore the gas lines leading into the reaction chamber had to be changed to metal as the ammonia was corrosive to the previous plastic line. Furthermore, since ammonia is toxic, a regulator with its own shut-off valve was added. This meant small regulated amounts of ammonia could be released into the reactor at a time. So if there was a leak present in the piping only a small amount would escape.

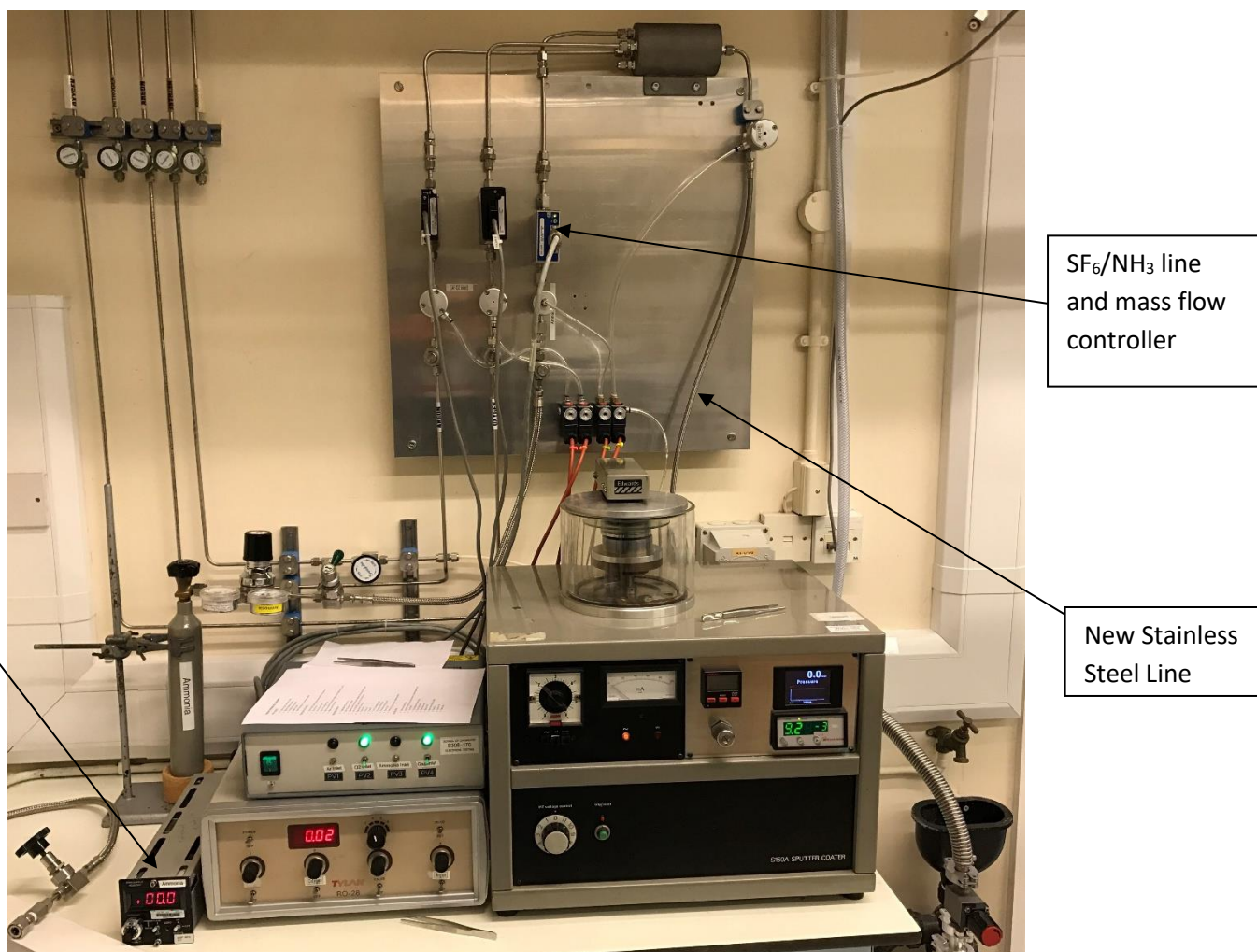


Figure 26: Image of the completed plasma reactor with the labelled changes

5.3.2 Gases Chosen for Termination

SF_6 gas was chosen for the fluorine termination since it gives a high atomic density of fluorine atoms. The density of fluorine atoms was found to be higher than other gases reported for fluorine termination, such as XeF_2 and CF_4 .

SF_6 has a large cross-section for dissociative attachment processes. This process results in SF_5^- and F^- species forming. The SF_5^- can then undergo several other dissociative attachment processes in order to produce additional F species. However, the successive dissociations have a lower rate since the cross-section decreases. This can be seen in the table below. These F species can undergo termination reactions on the diamond surface⁹⁰.

Reaction	Expected threshold energy (eV)	Measured ^a threshold energy (eV)
$SF_6 + e \rightarrow SF_5 + F + e$	9.6	—
$SF_6 + e \rightarrow SF_4 + 2F + e$	12.1	—
$SF_6 + e \rightarrow SF_4 + F_2 + e$	11.3	—
$SF_6 + e \rightarrow SF_3 + 3F + e$	16.0	16.0 ^b
$SF_6 + e \rightarrow SF_3 + F + F_2 + e$	15.2	
$SF_6 + e \rightarrow SF_2 + 4F + e$	18.6	19.5 ^b
$SF_6 + e \rightarrow SF_2 + 2F + F_2 + e$	17.8	
$SF_6 + e \rightarrow SF_2 + 2F_2 + e$	17.0	
$SF_6 + e \rightarrow SF + 5F + e$	22.7	22.0 ^b
$SF_6 + e \rightarrow SF + 3F + F_2 + e$	21.9	
$SF_6 + e \rightarrow SF + F + 2F_2 + e$	21.1	

Table 3: Expected or measured threshold energies for electron impact dissociation of SF₆ into neutral species⁹¹.

CF₄ produces a slightly lower number of F species however it was not chosen due to the fact that it results in the formation of carbon radicals that may react with the diamond surface resulting in sp² carbon being deposited.

Although nitrogen termination can be achieved through the use of N₂ gas, ammonia termination has only been reported with the use of NH₃ gas. This made it a clear choice for the reactor. An alternative method would have been using N₂ gas to achieve a nitrogen terminated layer and then using the hydrogen plasma reactor to change this into ammonia terminated diamond. However, there is a chance that the hydrogen plasma could remove some of the nitrogen-terminated surface.

5.3.3 Standard Operation of the Plasma Reactor

The HPHT diamond was placed in the middle of the anode before sealing the lid. The air inlet was closed and the rotary pump turned on to form an airtight seal. After a base pressure of 7×10^{-3} was established the desired gas was flowed into the system.

The different gases all required different conditions to strike a plasma. Pressure was controlled by the use of the needle valve on the rotary pump. The voltage was changed by a dial on the power supply. For all gases, the flow rate was kept constant at 10 sccm. The ideal plasma conditions for the gases are shown in the table below.

Gas	O ₂	NH ₃	SF ₆
Pressure (Torr)	0.1-1.5	1.3-1.6	0.1-0.3
Voltage (kV)	4-9	7-9	7-9

Table 4: Conditions for generating the O₂, NH₃ and SF₆ plasmas

These values were determined by altering the pressure and voltage until a continuous glow-discharge plasma was observed. Outside of these conditions the plasma would become less intense and flicker.

Prior research on oxygen terminated diamond surfaces using the reactor showed that etching occurred on the diamond surface after 10 s. SF₆ has been shown to have similar etching rates as oxygen and therefore initial sample measurements were based around this time. Ammonia was found to have a significantly lower etching rate and therefore the samples could be placed in the reactor for longer periods of time.

5.4 Emission Spectroscopy

Emission spectroscopy acts as one of the main plasma diagnostic methods. It allows for determination of the plasma composition without having an influence on the studied object. This method can allow for the determination of electron densities, temperatures and plasma composition. Optical emission spectroscopy (OES) was chosen for this experiment and it uses the visible part of the electromagnetic spectrum.

In the reactor the gas is ionized by the influence of a strong electric field. This results in the excitation of atoms or ions to higher energy levels. When the atoms or ions undergo a transition from that higher state back to a lower energy state, the excess energy is emitted as a photon. The energy of the released photon is the energy difference between the two states and is therefore characteristic of a specific molecule/atom. A spectrometer detects these photons which can then be used to diagnose the species in the reactor.

The emission spectra were recorded using an Ocean Optics USB2000+UV-VIS spectrometer. The spectrometer was capable of measuring wavelengths between 200 - 850 nm. The detector itself was a Sony ILX511B (2048-element linear silicon CCD array). It had a 25 μm slit with an optical resolution of 1.5 nm FWHM. The spectrometer also exhibits a signal-to-noise ratio of 250:1. A fibre optic cable was used to get light from the plasma reactor into the spectrometer.

5.5 Analysis of Functionalized Diamond Surfaces

5.5.1 Wettability

One of the simplest and quickest ways to differentiate between different diamond surfaces is through wettability, which is an indication of the thermodynamic properties of a surface. The different functional groups/atoms present on the diamond surface result in varying degrees of hydrophobicity. The resulting change in the shape of the liquid on the surface and is determined by the Young-Laplace equation (6)⁹².

$$\Delta p = \gamma \left(\frac{1}{R_1} + \frac{1}{R_2} \right) = 2\gamma H \quad (6)$$

This demonstrates the difference in capillary pressure, p , over a meniscus between two fluids. Additionally γ acts as the surface tension, H is the mean curvature, and R_1 and R_2 are the radii of curvature of the interface in orthogonal directions⁹³.

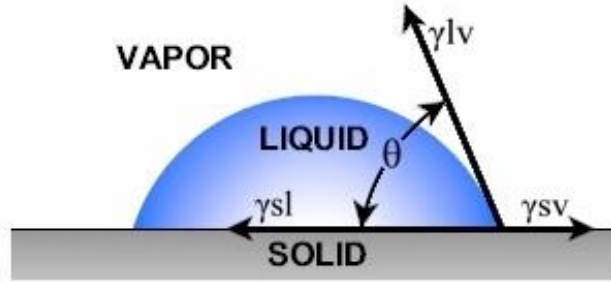


Figure 27: Schematic diagram that demonstrates Young's Equation⁹³

The sessile drop method can be used to quantify the change in the shape of the liquid by measuring the contact angle. This involves placing a drop of liquid onto the horizontal surface and measuring the angle, θ , between the surface and droplet.

$$\cos(\theta) = \frac{\gamma_{sv} - \gamma_{sl}}{\gamma_{lv}} \quad (7)$$

Here γ_{sv} , γ_{sl} and γ_{lv} are the interfacial tensions between gas-solid, liquid-solid and gas-liquid, respectively. Thermodynamic equilibrium conditions are assumed.

Salvadori et al have shown that fluorine-terminated diamond is the most hydrophobic surface with a contact angle of 107° . This was followed by hydrogen-terminated diamond and then oxygen-terminated diamond with contact angles of 70° and 47° , respectively. These angles vary for the degree of termination, however they can act as good indicators to see if a termination reaction has in fact taken place⁶⁵. Additionally, this method can result in highly reproducible results with an error of $\pm 1.2\%$ ^{94,95}.

Contact angle measurements are also sensitive to impurities and hysteresis. Additionally, water's hydrogen bonding nature can affect the reproducibility of contact angle measurements, since H_2O can stay chemisorbed to microcracks present in the surface.

The presence of varying groups on the oxygen-terminated diamond surface can affect the contact angle measurements. Ethers, carbonyls, lactones, carboxylic acids and hydroxyl groups all have varying degrees of hydrogen bonding and therefore will result in different contact angles.

5.5.2 Contact Angle Measurements

Measurements were taken using a Krüss Droplet Shape Analyzer (DSA). Deionized water droplets were used in the surface analysis measurements. The drops were placed in the middle of the diamond sample using a SciChem variable micropipette 0.5-10 μL . In order to measure the contact angle the sessile drop method was used.

The software used to determine contact angle, Advance, was provided by Krüss. The fitting method used to determine the contact angle was the Young-Laplace method. This method is based on an ideal sessile drop, where the curvature is affected only by the equilibrium between surface tension and weight.

As stated above, the Young-Laplace equation gives a relationship between radii of curvature, surface tension and pressure for a curved liquid surface

$$\Delta p = \gamma \left(\frac{1}{R_1} + \frac{1}{R_2} \right) \quad (6)$$

For a symmetrical drop which is used in the experiment, the Young-Laplace fit gives the best correspondence between theoretical and real drop shape. The program gave both the right-hand and left-hand contact angles. An average of both angles was taken and then an average of three runs was used to generate the contact angle value⁹⁶. An example of a generated image can be seen below.

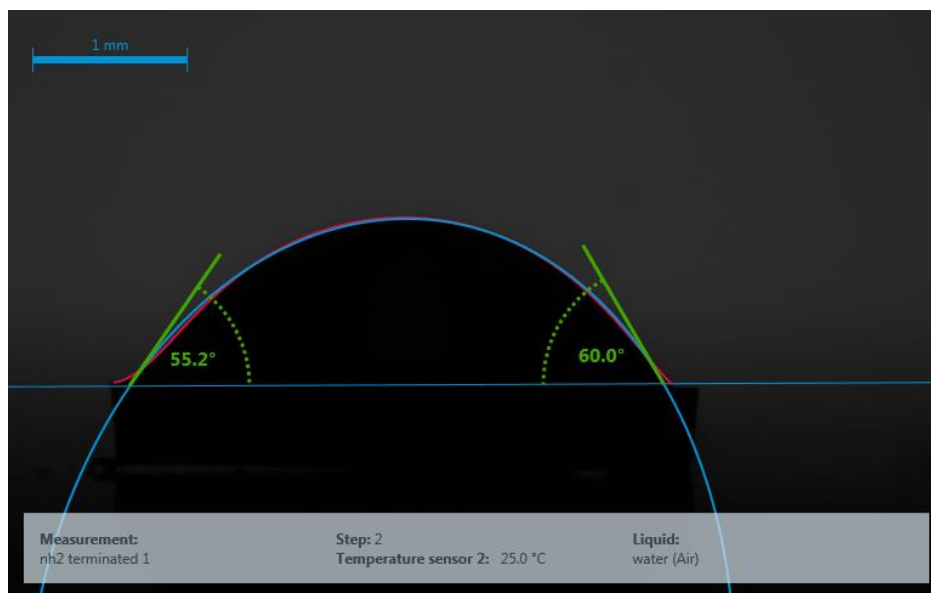


Figure 28: Image of the contact angle measurement generated by the Krüss Drop Shape Analyser with the use of the Advance program.

Prior to contact angle measurement, each sample was cleaned with ethanol and then dried by heating on a hot plate at 80°C for 15 minutes. The first contact angle was measured 3 s after the drop was placed,

with the next 2 contact angle measurements taken each after 1 s. This was done using the 20 FPS video feed on the machine.

5.5.3 X-Ray Photoelectron Spectroscopy

X-Ray Photoelectron Spectroscopy (XPS) is an ultra-high vacuum (UHV) process that can be performed by the NanoESCA facility present at Bristol University. The machine uses Al K_{α} X-rays with an energy of 1486.7 eV.

XPS is an application of the photoelectric effect, which is the emission of electrons or other free carriers when X-rays shine on a material. This therefore, requires a fixed monochromatic X-ray photon source. If the source is non monochromatic it will result in the peak broadening, appearance of satellite peaks and a higher background signal.

The technique can provide a quantitative characterization of the terminated diamond surface. The resulting spectrum is made up of emitted photoelectrons that vary depending upon their energy. Monoenergetic X-rays strike the surface, which results in the ionization of the surface atoms and the subsequent release of an electron in the process.



Ionising radiation can penetrate several microns. However, only electrons from the top few nanometres can escape the surface and are the ones that contribute to the XPS spectra.

The binding energy (BE) of the electron is characteristic of the atom since it arises from the core of the atom. Therefore, by measuring the kinetic energy (KE) energy of the emitted electron and using the equation below it is possible to determine the surface composition.

$$E_{X\text{-ray}} - KE = BE \quad (9)$$

XPS can also give information regarding the stoichiometric ratio among different elements. After discarding the background, one can calculate atomic concentrations from the peak intensities. This can be seen in figure 29 (B).

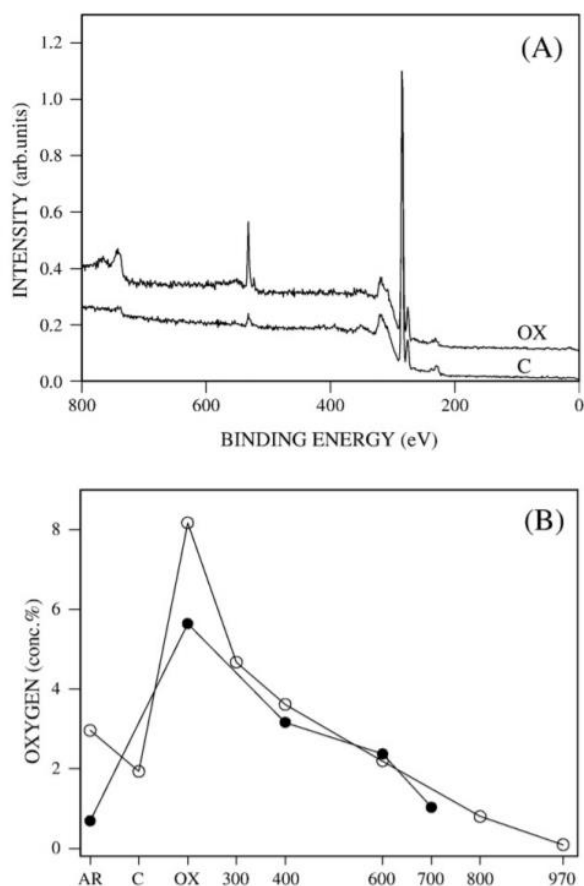


Figure 29: (A) XPS spectra of clean (C) and oxidized (OX) diamond. The peak at roughly 550 eV in the oxidized graph indicates the increase in oxygen on the diamond surface. (B) represents the oxygen concentration on the two samples which was calculated from XPS⁹⁷. On the x axis AR, C and OX represent: as received, cleaned and oxidized respectively. The subsequent numbers refer to different annealing temperatures.

As stated previously XPS is an UHV technique and these conditions result in the electrons mean free path length being several kilometres. This means that the electrons can easily travel from the sample through to the analyser and finally the detector. Moreover these ultra-low pressure conditions result in less contamination, as less molecules reach the sample surface over a given period of time. The UHV conditions are established by a series of pumps. Displacement pumps (rotary) bring the pressure down to 10^{-2} mbar. Following this momentum transfer pumps (turbomolecular) are used to reach high vacuum conditions. Finally entrapment pumps (titanium sublimation and ion pumps) bring the pressure down to the UHV region of 10^{-9} mbar.

Electrons were detected by an electron analyser. This separated electrons based on their KE. One of the most common types of analysers is the hemispherical analyser. Electrons travel between two concentric hemispheres. A potential is applied to the hemispheres which causes electrons to follow

circular paths. The radii of the paths depend on the KE of the electron entering the analyser. The potential of the hemispheres can be varied during analysis. This results in the spectra are seen in figure 28 (a). A schematic diagram of a typical hemispherical analyser can be seen below.

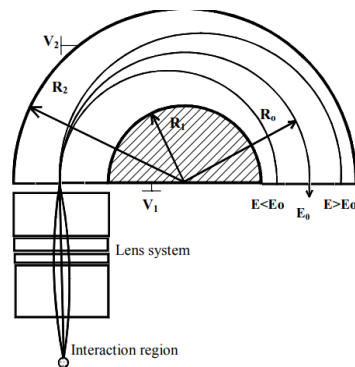


Figure 30: Schematic diagram of a hemispherical analyser⁹⁸

5.5.4 Scanning Electron Microscope

This technique is used to produce a high-resolution, 2- dimensional image of the surface. Electrons are rastered across the surface under high vacuum. Scanning electron microscope (SEM) can produce two different types of images. The first is through the reflection of low energy secondary electrons off the surface by inelastic scattering events. These electrons are reflected from the surface and accelerated towards a detector. This provides a better understanding of the morphology of the surface. The electrons are emitted very close to the specimen surface, which causes the high resolution. Images higher on the surface appear lighter than those further down. For SEM the secondary electron image is generally the most useful type for topographic analysis.

The second method is through backscattering which is when electrons from the beam re-emerge from the sample surface. These electrons contain less energy than those in secondary electron SEM. Backscattered images have lower resolution. This is because depth of backscattering electrons can be greater which hinders topographical resolution. However, backscattered electrons are more sensitive to atomic mass as heavier atoms will scatter more electrons back to the surface. This means these heavier elements will appear brighter on the generated image. This can be illustrated in figure 31.

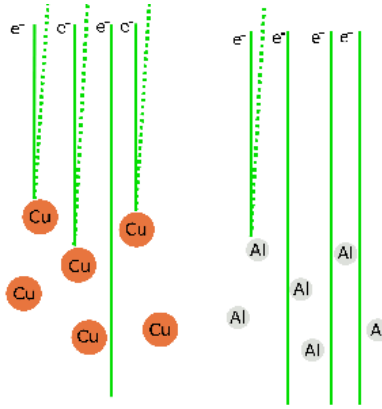


Figure 31: More electrons are reflected off the heavier Cu atom in backscattered SEM.

The resolution and depth of the image produced depends upon the acceleration of these electrons. This can be shown in the following equations.

$$\frac{1}{2}mv^2 = eV = \text{KE} \quad (10)$$

Here kinetic energy is given in terms of: mass (m), velocity (v), electron charge (e) and voltage (V). Electron velocity can also be given in classical terms using momentum (p) and mass as seen in the equation below.

$$v = \frac{p}{m} \quad (11)$$

The de Broglie relationship relates a moving particles wavelength with its momentum as shown below.

$$p = \frac{h}{\lambda} \quad (12)$$

Using this, a new equation for wavelength can be given. Due to wave-particle duality the wavelength relates to the resolution of the image.

$$\lambda = \frac{h}{\sqrt{2meV}} \quad (13)$$

The resolution can be limited by the electron probe diameter. The narrow electron beam in SEM results in a large depth of field which yields a characteristic 3D appearance⁹⁹.

SEM images were obtained using the Jeol IT300 SEM operating at 15 kV. It can provide magnification between $\times 5$ to $\times 300,000$. Electrons are generated through the use of a pre-centred tungsten hairpin filament. The secondary electron (SE) resolution mode was between 3.0 nm (30 kV) to 15.0 nm (1.0 kV). The backscattered electron resolution mode was 4.0 nm (30 kV). An image of the machine can be seen in figure 32.

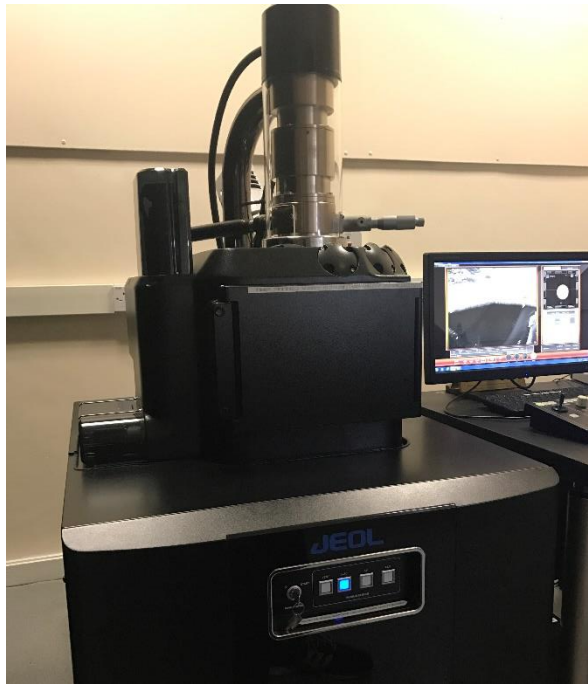


Figure 32: Photograph of the JEOL IT 300 SEM.

6. Results and Discussions

6.1 Optical Emission Spectroscopy

OES was used to diagnose the species that were generated by the plasma reactor. The species present in tables below were detected by the spectrometer.

Molecule	Transition	Literature Wavelength (nm)	Experimental Wavelength (nm)	Intensity (a.u)
SF _x	Band	289	292.16	15000
F	$3p^2F_{7/2}^0 \rightarrow + 3s^2$ D _{5/2}	730.9	732.11	32000
F	$3p^2P_{1/2}^0 \rightarrow 3s^2P_{3/2}$	703.7	705.12	26000

Table 5: The experimental and literature values of the species observed by OES in the SF₆ plasma

Molecule	Transition	Literature Wavelength (nm)	Experimental Wavelength (nm)	Intensity (a.u)
NH	A ³ Π→X ³ Σ	337	331.44	20000
H	H _α	656.28	655.31	40000

Table 6: The experimental and literature value of the species observed by OES in the NH₃ plasma

The ammonia plasma generated two distinguishable species, the NH radical present at 331.44 nm and the H_α peak present at 655.31 nm. The plasma decomposition should have resulted in two additional primary products (NH₂ and H₂) that did not appear. However, these peaks tend to have far lower intensities and are hard to distinguish in the spectra due to the background interference.

Moreover secondary reactions should result in the formation of N₂, N₂H₂, and N₂H species. Species that contain two nitrogen atoms are found to increase with power (400 W) and substrate heating temperature (900 K). This reaction was done at similar power but much lower temperatures. Therefore

the fact that we could not identify any species containing multiple nitrogen atoms can be attributed to this.

The identification of the NH species in the plasma is important since it will result in the desired ammonia termination. Furthermore, since NH and not NH₂ was detected it means that we will be more likely to see imines and secondary amines present on the surface as these are the two species the NH molecule can form¹⁰⁰.

Since different atoms/molecules emit light differently intensity cannot be considered to be a measure of concentration. Therefore it is hard to tell how much of each species we are generating. Therefore in the case of the ammonia plasma we could be generating more H than NH which means hydrogen termination could occur in the reactor.

For the SF₆ spectra two separate fluorine transitions were observed as well as an SF_x band. A typical SF₆ spectra shows several peaks between 680 - 810 nm, which relate to F transitions. Two of these peaks were identified as the $3p^2F_{7/2}^0 \rightarrow + 3s^2 D_{5/2}$ transition at 732 nm and the $3p^2P_{1/2}^0 \rightarrow 3s^2P_{3/2}$ transition at 705 nm. The SF_x band transition was identified at 292 nm. The appearance of the SF_x band is important since it means that the formation of the fluorine atoms is occurring through dissociative attachment which generates SF_x and F species. However as the concentration of the F atoms is not known it is hard to determine the extent of the dissociative attachment process and thus the number of F atoms generated per SF₆ molecule.

We must consider the fact that these results may not be entirely accurate due to the fact that the light emitted by the plasma could not be isolated due to the borosilicate shield around the reaction chamber. Therefore, there was a large amount of background noise present between 400 - 600 nm which made other signals difficult to identify.

6.2 Contact Angle Measurements

6.2.1 Ammonia Termination

Initially, contact angle measurements were used as an indication as to whether the surface had undergone a termination reaction. Deionized water droplets of size 0.35 μL were used to perform the measurements. For all the ammonia-terminated samples the pressure and voltage in the reactor was kept constant at 1.6 Torr and 8 kV, respectively. The amount of time the ammonia was exposed to the plasma was varied from 0 to 150 s, in 30 s intervals. The results can be seen in the graph below.

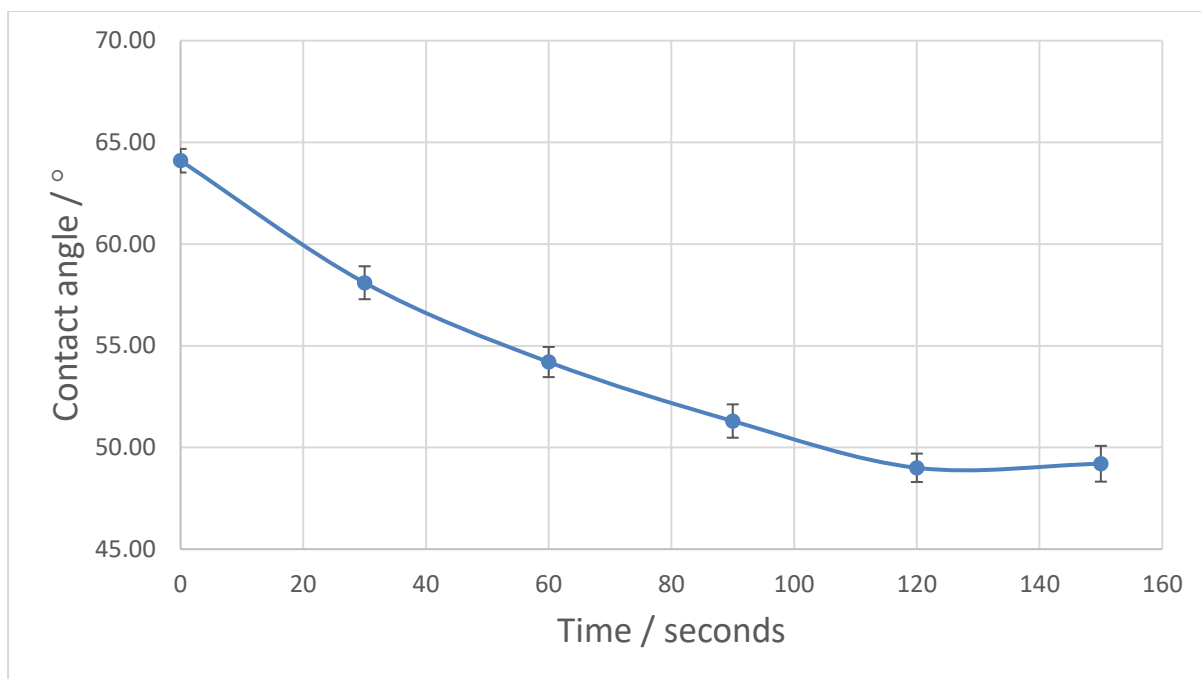


Figure 33: The change in contact angle with an increased exposure to the ammonia plasma

A decrease in contact angle indicates a decrease in hydrophobicity. This acts as a good indication that some degree of ammonia termination has occurred on the surface as NH_3 -termination will result in a more hydrophilic surface.

After 120 s the contact angle stopped decreasing. This was assumed to be the point where maximum coverage possible by the plasma reactor was achieved. Additionally, unlike oxygen termination, after the minimum there was no increase in contact angle due to etching of the diamond surface. This is expected as an ammonia plasma does not have as high an etching rate as an oxygen plasma.

6.2.2 Fluorine Termination

For SF_6 , pressure (0.1 torr) and voltage (8 kV) were kept constant for all the samples. The amount of time the diamond samples were exposed to the plasma was varied from 0 to 30 s, in 10 s intervals. The time intervals for the SF_6 treated samples were lower due to the plasma having a high etching rate. The droplet used was deionized water with a volume of 0.35 μl . The results can be seen in the graph below.

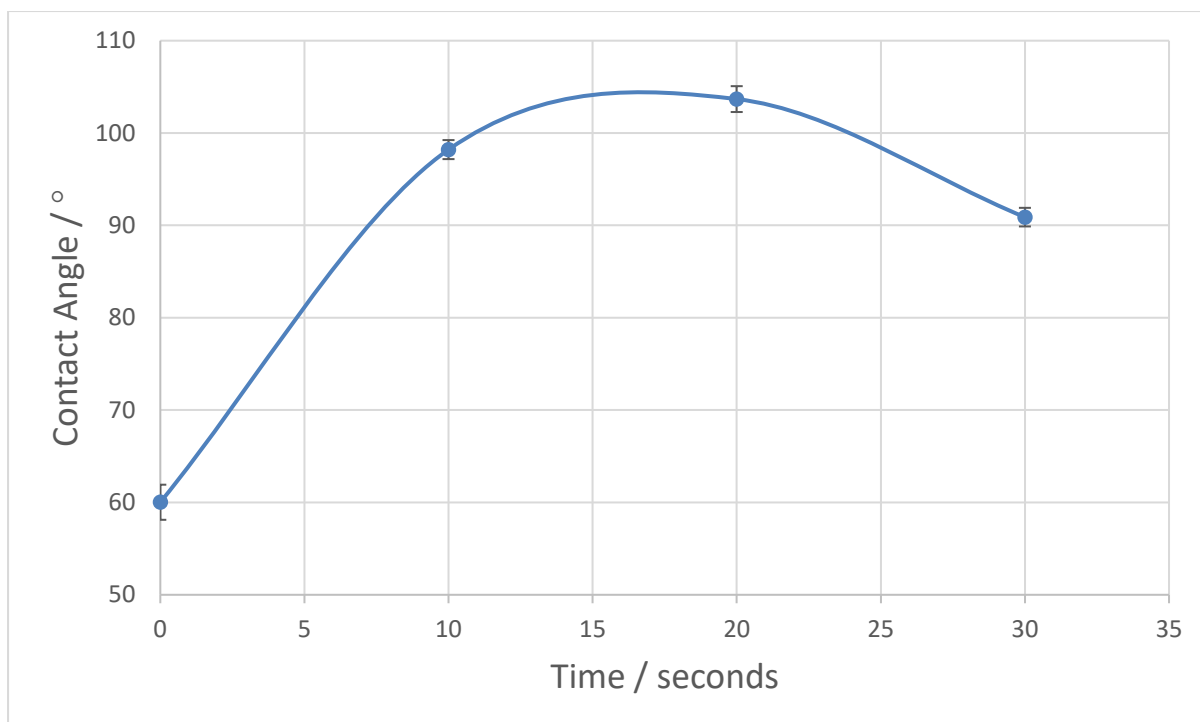


Figure 34: The change in contact angle with an increased exposure to the SF₆ plasma

Since the F-terminated diamond surface is more hydrophobic than the starting H-terminated diamond surface, the plasma exposure time was increased until a maximum was found. This maximum in the curve occurred at about 20 s. After this point, the contact angle began to decrease. This could be a result of damage to the diamond surface. One possible example could be etching which has been found to affect surface roughness and thus contact angle. Therefore, 20 s was assumed to give the best possible F-termination without compromising the surface.

It is however important to note that in the case of oxygen termination, etching was found to increase the contact angle. If etching did in fact occur on the diamond then the contact angle should have continued to rise. The sudden decrease in contact angle could therefore be the result of something else. Therefore, SEM analysis was performed in order to see how the surface changed and will be discussed later on as a way to try and rationalize this observation.

Further research can be performed to find a more precise termination time. Measurements with 1 s intervals should be taken between the 10 and 20 s region in order to see if a higher contact angle can be achieved. However, due to a limited number of samples this was not done and 20 s was assumed to give the best possible termination.

6.2.3 Comparison of contact angles

The graph below shows the contact angle of the samples at what is assumed to be at the highest coverage of their respective termination. Oxygen terminations were performed in order to make sure the reactor could still successfully carry out this procedure. The sample was exposed to the O₂ plasma for 7 s at a voltage of 8 kV and a pressure of 0.1 torr. These conditions were reported to give a monolayer of coverage⁸⁹.

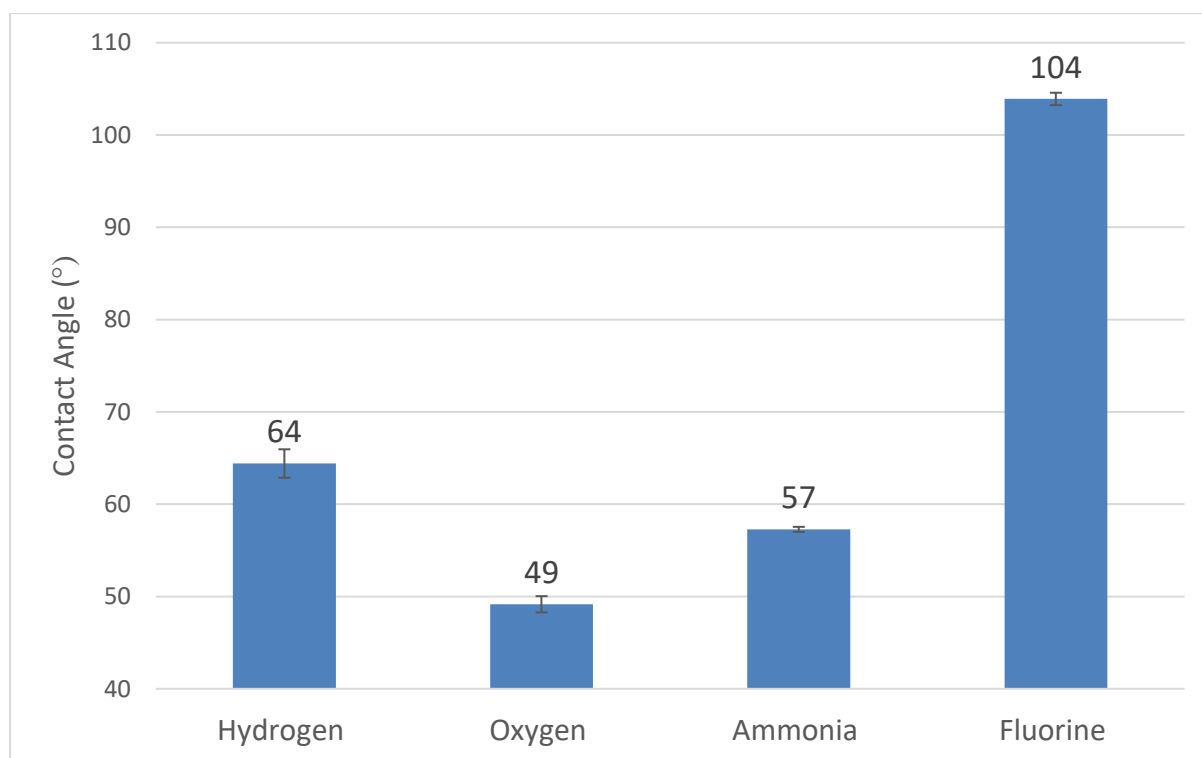


Figure 35: The contact angle of the hydrogen, oxygen, ammonia and fluorine-terminated diamond surfaces

The literature showed that the contact angle for fluorine-terminated diamond should be 107° ⁶⁵. This value we achieved was $104^{\circ} \pm 0.7^{\circ}$. For oxygen-terminated diamond the literature value was found to be 47.2° ⁶⁵, whereas the experimental value was found to be $49 \pm 0.9^{\circ}$. This difference in contact angle could be attributed to the fact that we may have not been able to achieve an ideal coverage of a monolayer with the reactor. Alternatively, as the literature samples were performed on CVD diamond their samples may have a different roughness which would result in different values of contact angle, even if both of the surfaces are fully terminated. However, it is important to note that the difference between both values and their literature is relatively low. Thus, the samples can be thought to have close to an ideally terminated surface.

The value for the ammonia contact angle should be closer to that of oxygen one due to the similar electronegativity. The literature states a value of 51.3° for NH₃-terminated diamond. This difference

could be due to the fact that only some of the surface was terminated in ammonia groups whilst the rest of the diamond surface remained hydrogen terminated. This would explain why the value is so high ($57^\circ \pm 0.9$) and closer to the value for hydrogen (64°).

6.3 XPS

XPS was performed in order to find out the quantity and nature of the elements present on the diamond surface. Unfortunately, due to the lack of availability of the NanoESCA and the time constraints of the project, XPS analysis was only performed on the NH_3 -terminated surfaces.

6.3.1 Ammonia Termination

The survey scan (figure 36) of the 2 min NH_3 -terminated sample showed a large number of impurities present on the surface. Additionally, it also indicated the presence of both nitrogen and oxygen groups.

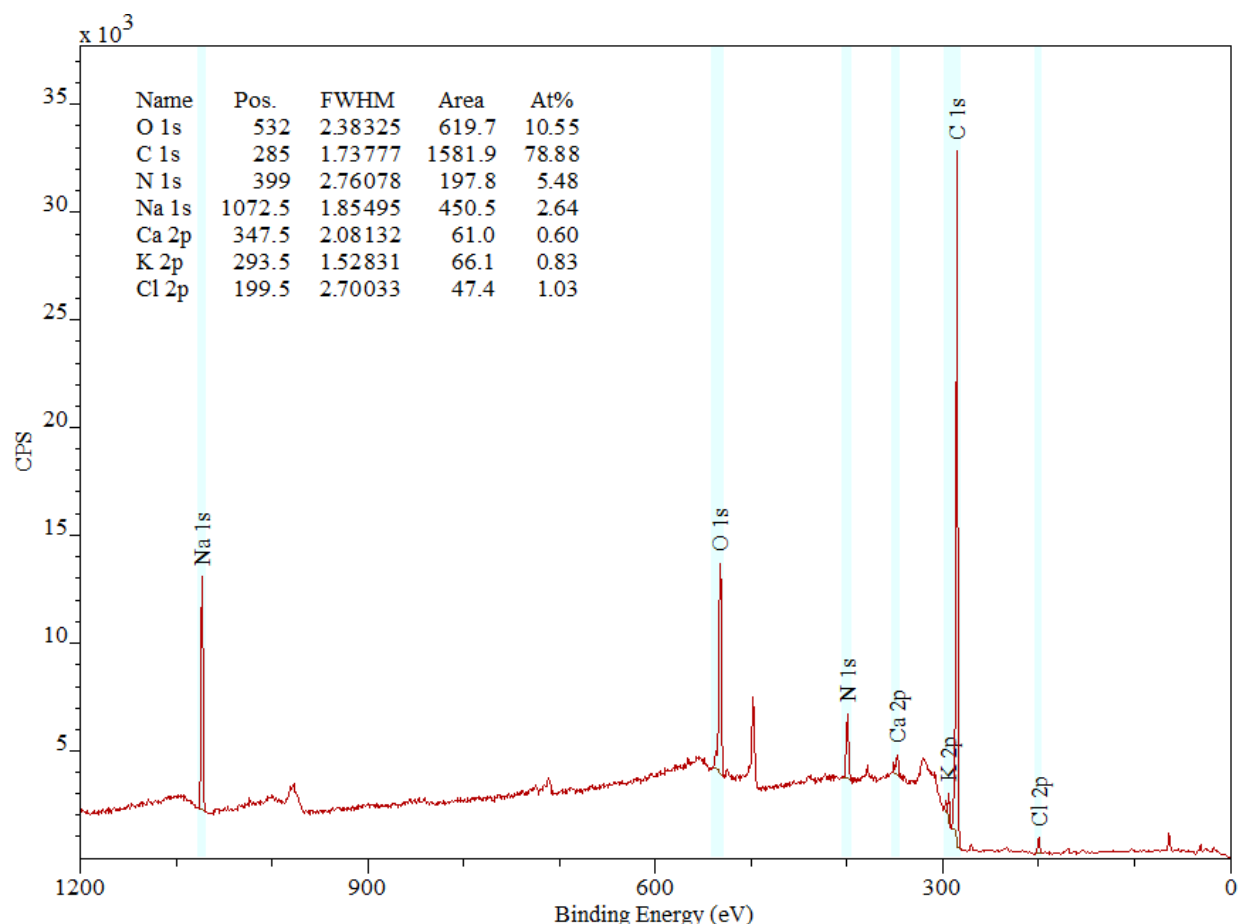


Figure 36: Survey scan of the initial 2 min NH_3 terminated sample.

The presence of the large oxygen peak can be attributed to the fact that the hydrogen termination is unstable and will oxidize in ambient conditions over time. Since the H-termination was performed about 2 months prior to the exposure to the ammonia plasma, the H-terminated surface slowly oxidized over

time. The surface was also found to contain 10.55% oxygen. Previous studies showed that one monolayer roughly relates to about 6%. This suggests there are almost two monolayers of oxygen present on the surface.

Despite the large amount of oxygen present there is also 5.5% nitrogen on the surface. This should roughly translate to a monolayer of coverage. This is a good indicator that the ammonia plasma can deposit nitrogen on the surface. Moreover, the fact that the nitrogen termination was still present means that it is relatively stable. Hydrogen doesn't show up on the XPS scan, as it has no core electrons, this means that it is difficult to differentiate between nitrogen and ammonia termination. However, we can look at the N1s binding environment to see what type of nitrogen groups are present.

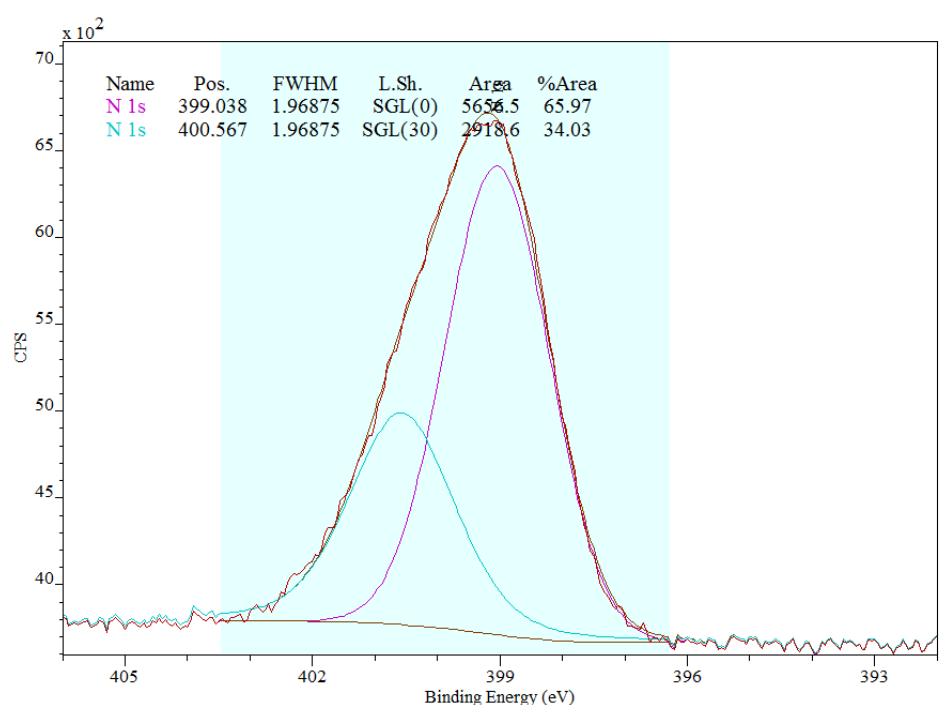


Figure 37: N1s binding environment in the initial 2 min NH₃-terminated sample.

The figure above is of the N1s binding environment. There are two separate components that make up the peak, one at 398.8 eV (imine) and another at 400.7 eV (secondary amine). This means that on the diamond surface both of these functional groups are present. Both these peaks suggest that the surface is in fact NH₃-terminated opposed to just nitrogen.

This agrees with the literature that states for a (100) diamond surface both imine and secondary amine groups should be present. Moreover, the OES indicated the formation of NH molecules in the plasma. This species would result in both secondary amine and imine formation which is consistent with the XPS data.

The C1s environment (figure 38) can be used to see if the nitrogen and oxygen monolayers are stacked on top of one another or if the surface is multi-terminated. The scan contains components for both nitrogen (C=N 285.9 eV) and oxygen (C-O 285.8 eV) which means that the oxygen and nitrogen monolayers are not stacked on top of one another, but instead the surface is multi-terminated with regions of oxygen and nitrogen with several monolayers of atoms in these regions^{101,78}.

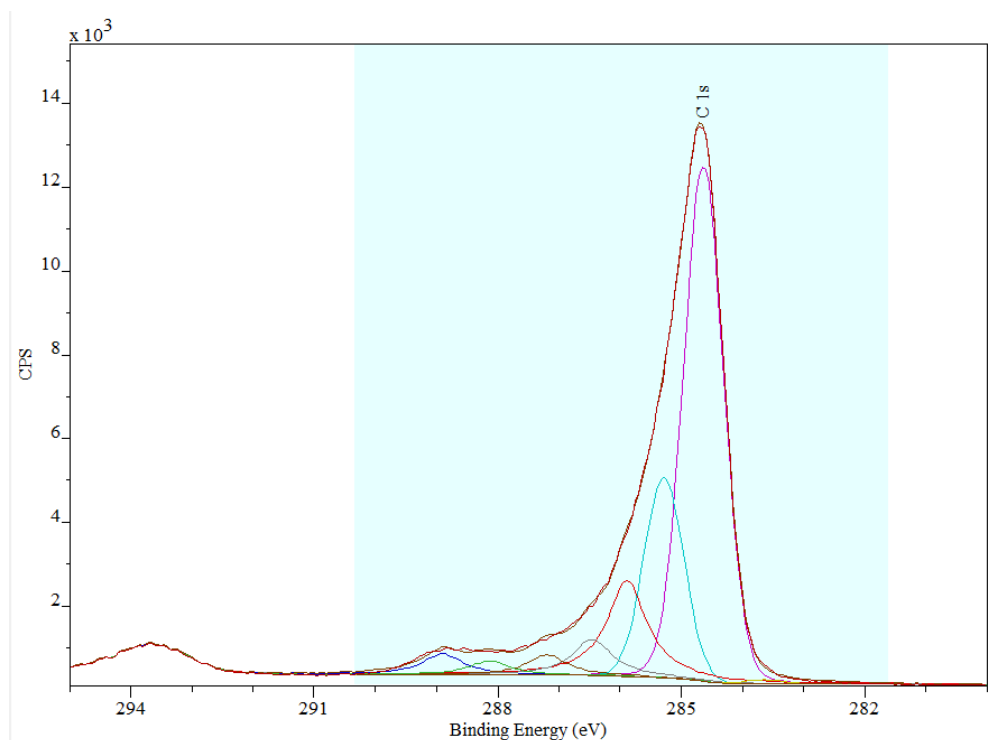


Figure 38: C1s binding environment in the initial 2 min NH₃-terminated sample

The other impurities: sodium, calcium, potassium and chlorine could all be present from the contact angle measurements. This means that the ethanol and water clean may not be sufficient in removing all surface impurities. The fact that there was a 2:1 ratio of oxygen to nitrogen on the surface means that surface cannot be considered to be ammonia terminated. Additionally, this could be the reason the contact angle values did not match the literature as a multi-terminated surface could affect the shape of the water droplet.

We can also look at the O1s binding environment (figure 39) to see the groups present. The O1s binding region is more complicated than that of the N1s region. It is comprised of two separate peaks and 3 components. The two components in the first peak relate to the ether (530.6 eV) and ketone (533 eV) binding environment. The second peak (536 eV) could be related to the interaction of the oxygen with nitrogen, as this has been found to occur at 536.2 eV for N-O on Al. However a peak for the N-O interaction doesn't show up in the nitrogen region of the survey scan. This indicates the peak could be the result of another interaction, such as oxygen with one of the impurities.

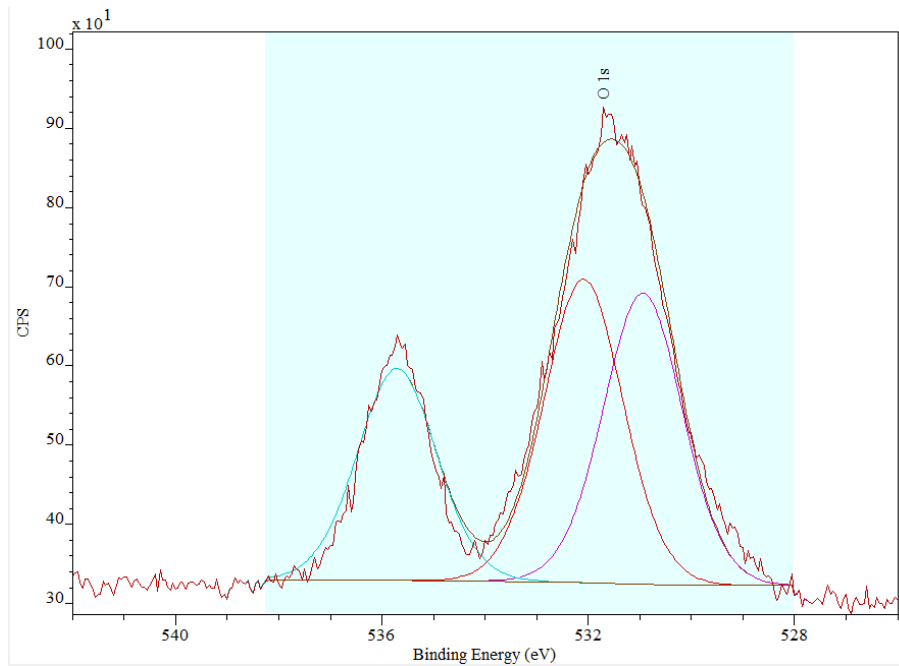


Figure 39: O1s binding environment in the initial 2 min NH₃-terminated sample

In order to see if the areas and the several monolayers in the first scan could be reproduced, a sample that was previously oxygen terminated underwent a nitrogen termination. The survey scan is shown in figure 40.

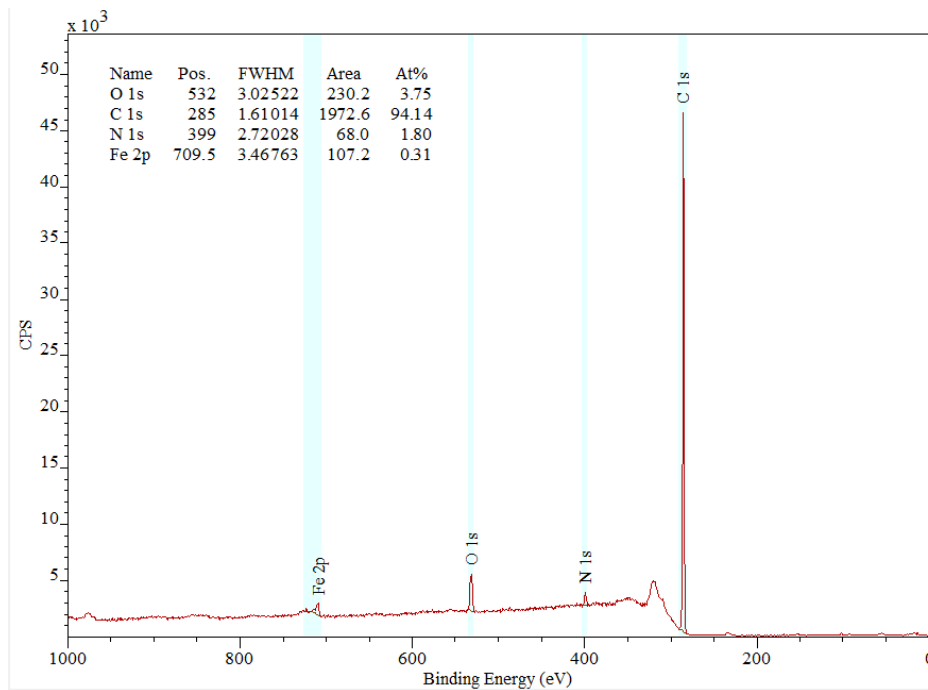


Figure 40: Survey scan of a sample that was oxygen terminated and then exposed to an ammonia plasma for 2 mins

In this sample the ratio of oxygen to nitrogen peaks is 2:1 which is the same as that found in the first sample. This suggests that the ammonia plasma is less efficient in terminating the sample than the oxygen one. Furthermore, since the ratio is the same it may mean that percentages in the first sample may have been inflated, due to the other impurities. Since the impurities are most likely oxidized it could have resulted in an increase in oxygen concentration. This means that there were not several monolayers of NH_3 and O. Furthermore, the sum of the nitrogen and oxygen coverage equals 5.55%. If we include the Fe impurity the total increases to 5.86% which is a monolayer on the surface.

In order to achieve a cleaner surface and remove any impurities, the samples underwent another H-termination. Immediately after the H-termination the samples were terminated again for 1 and 2 mins in the ammonia resulting in the survey scans below.

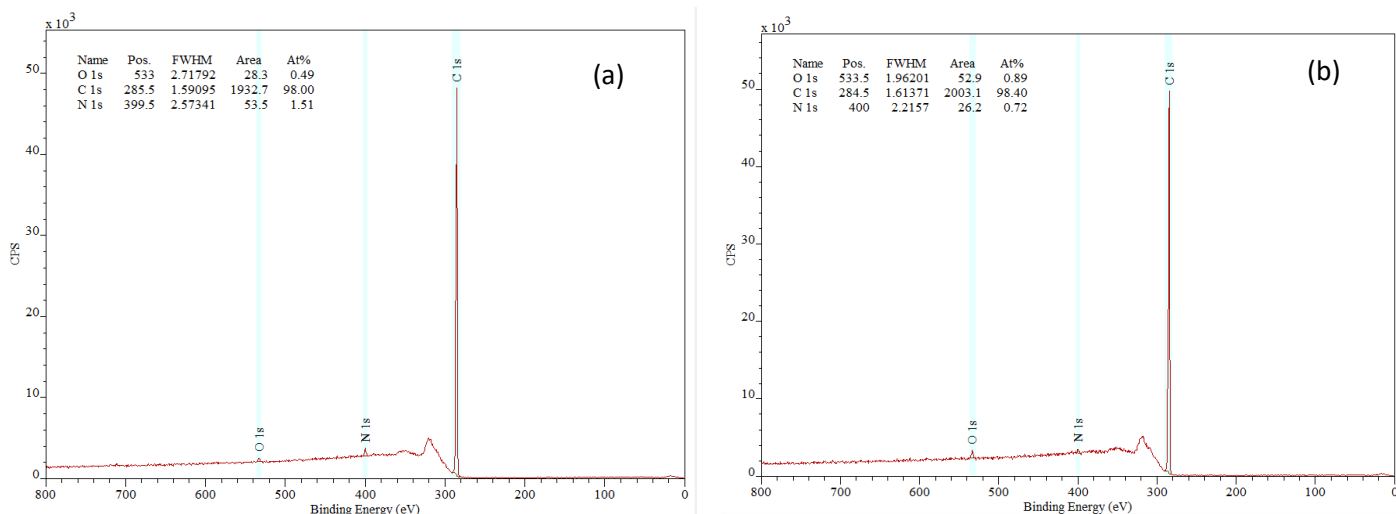


Figure 41 (a): Survey scan of the 1 min NH_3 -terminated sample. **Figure 41 (b):** Survey scan of the 2 min NH_3 -terminated sample.

The 1 min sample showed a greater percentage of NH_3 -termination in comparison to the 2 min sample. This is surprising as increased plasma exposure should not cause a decrease in termination. The values for the area have an error associated with how well they are fitted which could be the reason for a difference. However the nitrogen peak is visibly smaller in the 2 minute survey scan.

In order to see if the result was a possible anomaly, two more samples were terminated in the ammonia reactor for 30 s and 3 mins, respectively. The resulting survey scans can be seen in figures 42 (a) and (b).

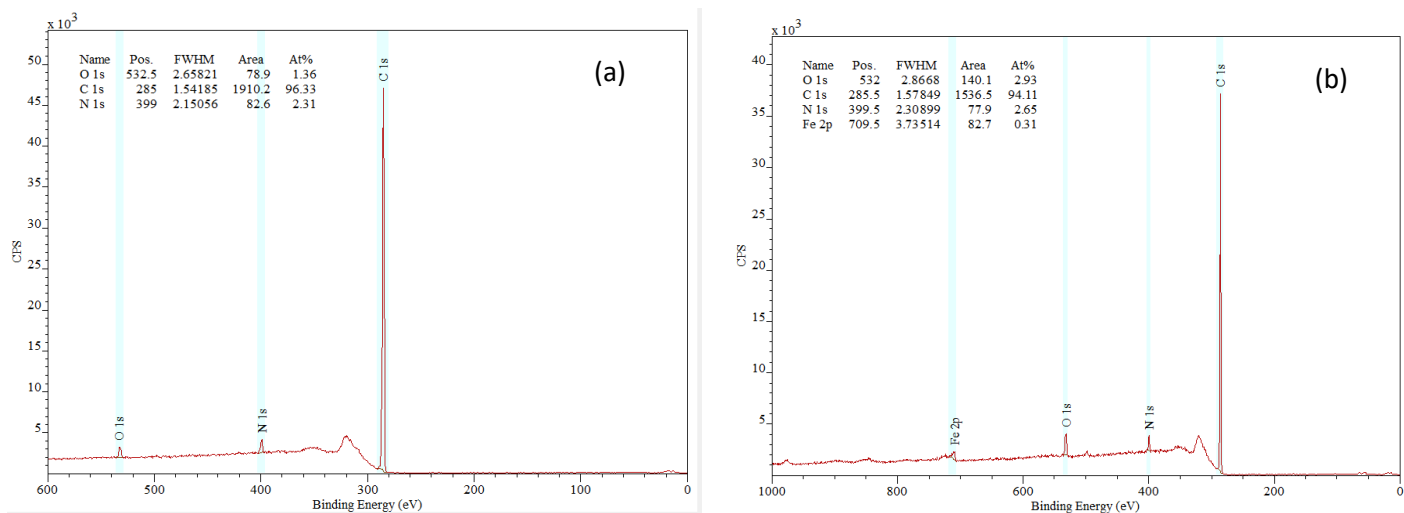


Figure 42(a): Survey scan of the 30 s NH₃-terminated diamond sample. Figure 42(b): Survey scan of the 3 min NH₃-terminated diamond sample.

Unfortunately, these samples could not be analysed immediately in the XPS and were left under ambient conditions for 3 weeks. This resulted in oxygen peaks present in both of the survey scans, due to the oxidation of the hydrogen-terminated regions. Alternatively, some of the oxygen could be present from OH molecules in the atmosphere replacing the NH molecules in an S_N1 reaction.

In both the 30 s and 3 min samples the ammonia terminations were relatively similar (2.5%, 0.4 ML) and greater than those present in the 1 min and 2 minute samples. This could be due to the fact that the ammonia gas line may not have been flushed out properly for the 1 and 2 min samples. Additionally, prior to the preparation of the 30 s and 3 min samples a leak test was performed and a small leak was found in the gas inlet line. Both these factors could have resulted in a lower percentage of NH₃-termination for the 1 and 2 min samples.

The survey scans suggest that that the maximum amount of NH₃-termination may have been possible after 30 s not after 120 s, which the contact angle measurement indicated, since the two samples have a similar percentage of NH₃-termination. The reason for the plateau could be due to the steric hindrance of the hydrogen atoms already present on the (100) surface and the incoming NH species. Moreover, the NH species are larger in size and therefore a full monolayer coverage may not be achievable. This means the remaining 60% of the surface is a mixture of oxygen and hydrogen-terminated diamond.

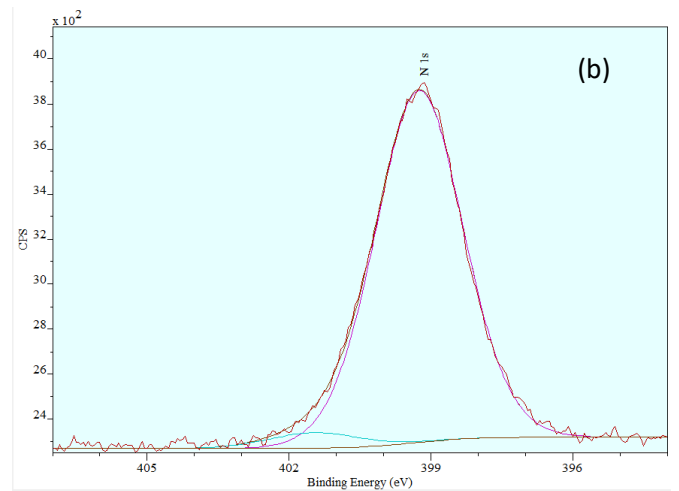
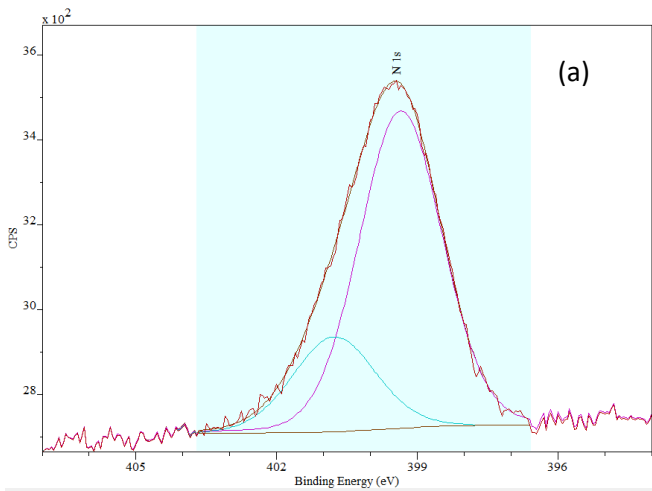


Figure 43: N1s binding environment in the 30 s (a) and 3 min (b) NH_3 -terminated samples.

If we compare the N1s binding environment of the 30 s and 3 min samples we see that there is an increase in the imine environment (398.8 eV). This implies that an increased plasma exposure results in a preferential deposition of the imine species. This has not been reported in the literature, however, in the case of oxygen termination, increased plasma exposure on the (100) surface was found to preferentially deposit ketone groups ($\text{C}=\text{O}$). Therefore a similar process may occur for NH_3 -termination where there is a preference for imine groups ($\text{C}=\text{N}-\text{H}$) with increased plasma exposure. This increase in imine groups could result in a reconstruction of the diamond surface which may, in turn, allow for the slightly higher coverage seen in the 3 min sample, 2.65%, compared to 2.31% in the 30 s sample.

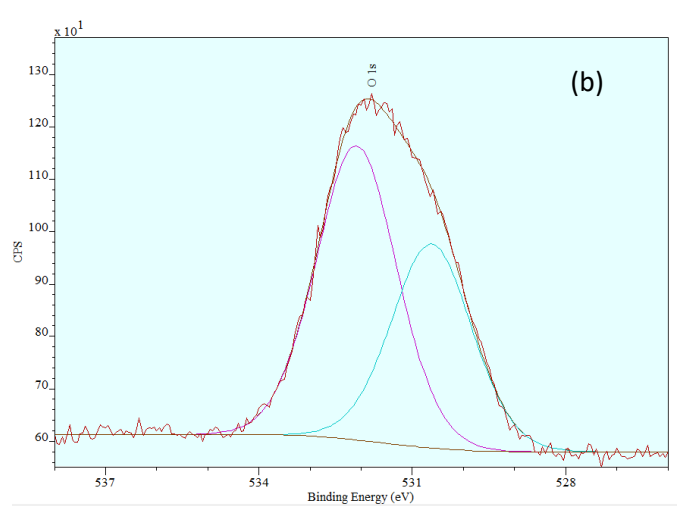
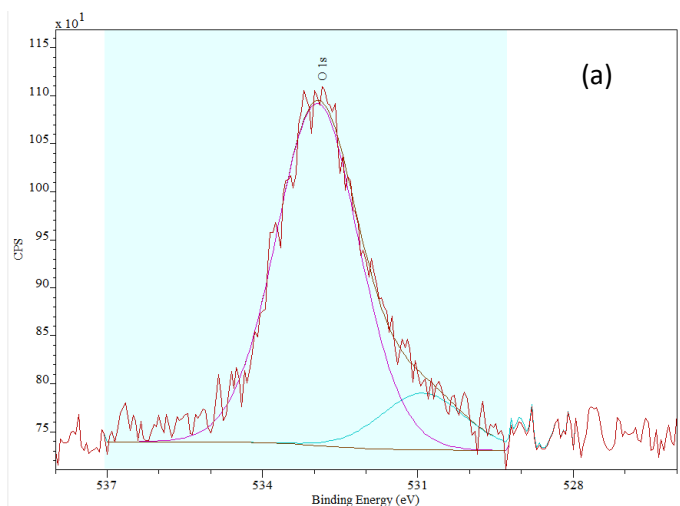


Figure 44: O1s binding environment in the 30 s and 3 min NH_3 -terminated sample.

The O1s binding environment in the 30 s and 3 min samples (Figure 44 (a and b)) also show a difference in the component peaks. In the 30 s sample the ketone (533 eV) environment is the dominant one, whereas for the 3 min sample the ketone peak is still larger, however the ether (530 eV) component contributes more to the peak shape. This could be a result of the increase in imines present on the surface which forced the oxygen terminated regions to rearrange from ketones to ethers. Moreover, in these scans there is no second peak like the one found in the first sample (figure 39), which confirms that it was a result of the oxygen atoms interacting with one of the impurities.

6.4 SEM

Backscattered and secondary electron SEM analysis was performed on the 30 s F-terminated sample. This was done in order to see if etching was the reason the contact angle began to decrease after 20 s of termination time. Unfortunately, we were not able to obtain images of a smooth HPHT sample prior to plasma exposure to compare these images with.

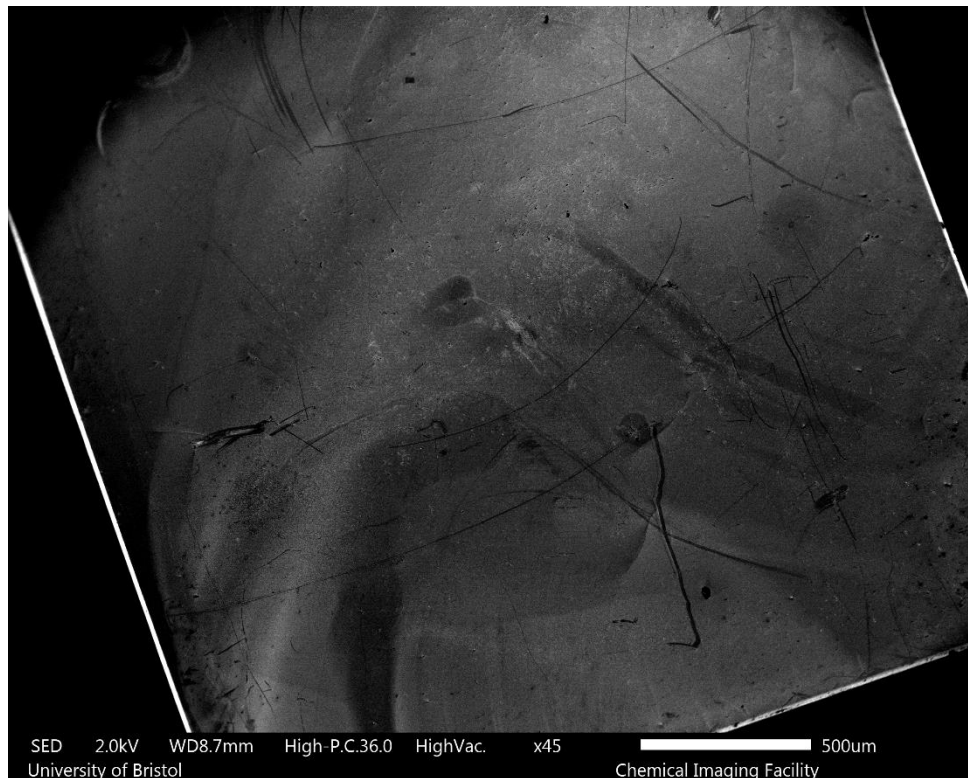


Figure 45: A SEM image of the entire HPHT diamond surface taken with $\times 45$ magnification.

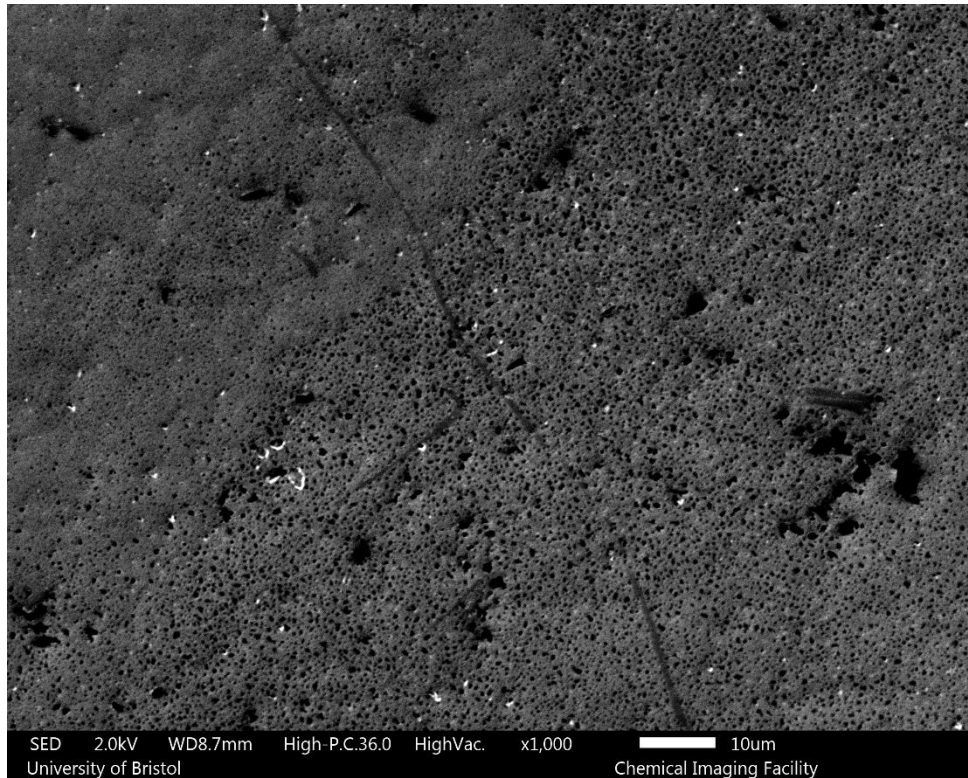


Figure 46: A SEM image of the diamond surface taken with a $\times 1000$ magnification.

Figures 45 and 46 are both SEM images of the diamond surface. Both these images indicate that the SF_6 plasma treatment damaged the sample. In the first image (figure 45) this can be seen by the scratches present on the surface. The lines vary in depth which means that the surface was not etched uniformly. It is also important to note that there doesn't seem to be a pattern in the etching of the surface.

Fig. 46 is at a higher magnification. Single-crystal HPHT diamond should have a uniform smooth surface. However, in this image one can clearly see that the morphology is varied across the surface. Again, this shows that the plasma did not etch the surface uniformly since there are darker areas with increased depth. This will increase the surface roughness which should have resulted in an increase in the contact angle of the diamond surface, not a decrease, which is what the results showed. However, the presence of holes in the diamond surface means that the water droplet may enter these areas causing the contact angle to appear more spread out over the surface. However, the holes would have to have a large area for the effect to be significant. This can be shown in figure 47 below.

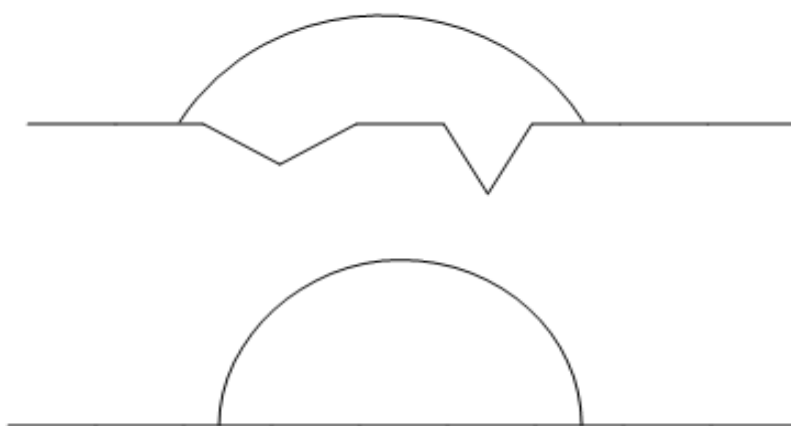


Figure 47: Image of how holes present on the surface can affect the shape of the water droplet.

In order to see if these etched regions were still carbon, secondary electron and backscattered images were taken of the same region with a higher magnification of $\times 1500$. Figure 48 (a and b).

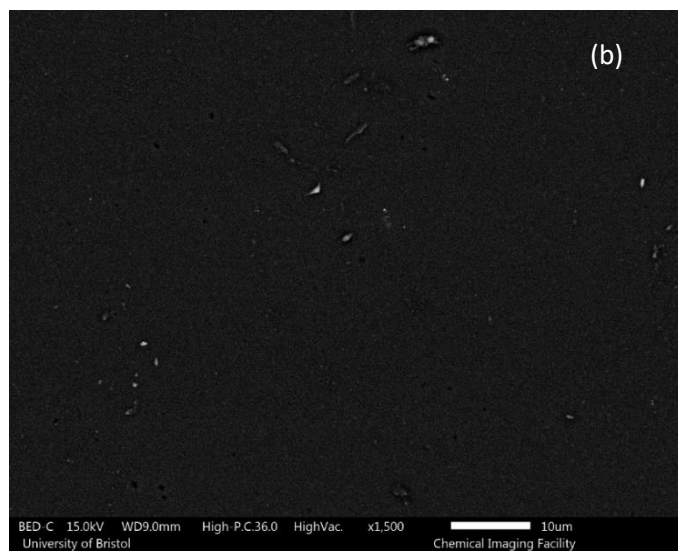
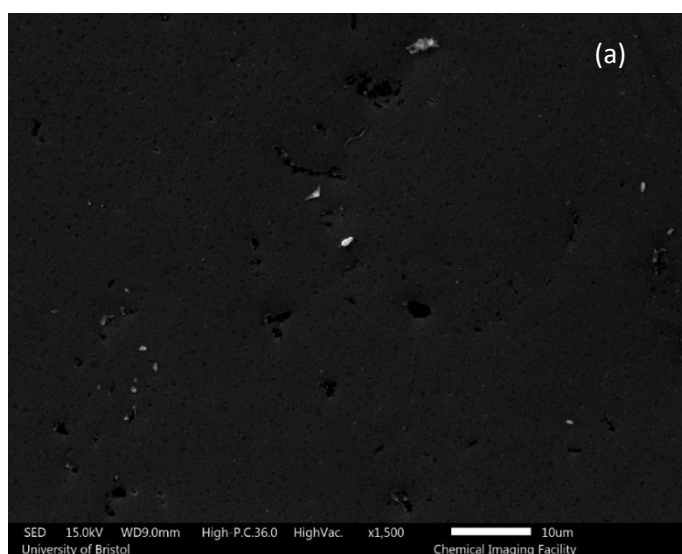


Figure 48 (a and b): Secondary electron and backscattered images of the same diamond surface at a magnification of $\times 1500$.

The darker areas in the previous secondary electron SEM image do not appear on the same backscattered image. This means that they are the same element as the rest of the material (carbon). The lighter regions appear in the same area for both SEM images. This could be areas of fluorine termination since they are heavier than the carbon atom and will scatter more light back, appearing brighter on the surface.

However, since fluorine is not significantly heavier than carbon the difference in brightness should not be as pronounced as it is on the image. Moreover, the size of the spots are fairly large which means that it is unlikely to be individual F atoms but possible regions of F-termination. The other more likely scenario is that it could be impurities adsorbed onto the diamond surface.

The final images were taken with a magnification of $\times 7000$. This was done to see if fluorine termination could be seen on the diamond surface. Secondary electron and backscattered SEM images were taken at this magnification.

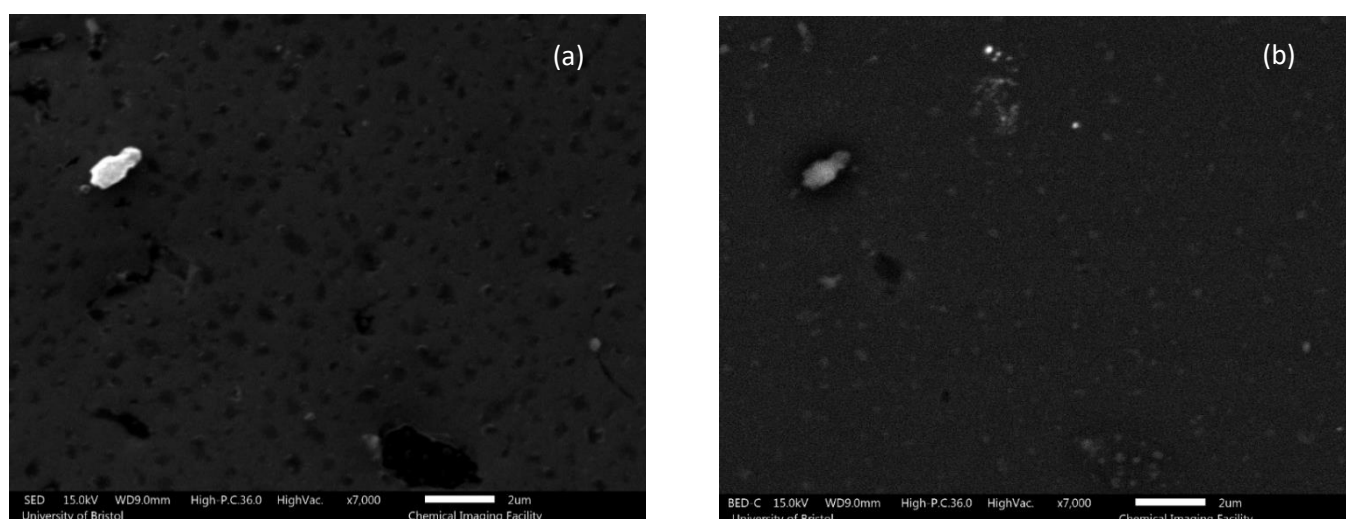


Figure 49 (a and b): Secondary electron and backscattered SEM images of the same diamond surface at a magnification of $\times 7000$.

These images indicate the possibility fluorine termination on the diamond surface as well as etching. On the secondary electron image we can see darker patchy areas that do not show up on the backscattered image, again suggesting the possibility of etching by the plasma. Moreover, the backscattered image also shows the presence of another element on the surface, as indicated by the white spots. This could potentially be fluorine atoms on the diamond surface, as the spots are far smaller and less bright than those seen in the $\times 1500$ images.

It can also be noted that the darker patches in the secondary electron image still show white spots on the backscattered SEM. This implies that even etched regions in the diamond could exhibit fluorine termination. These etched regions could have different surface structures, (111) for example. However, without XPS data it is not possible to say whether these spots are indeed fluorine atoms.

7. Conclusions

There were two different parts to this project: the construction of the reactor to aminate and fluorinate the diamond surface, and the analysis of the resulting surfaces.

Optical emission spectroscopy was the first analytical technique used to diagnose the plasmas generated by the reactor. For the NH_3 plasma, species relating to NH and H were found. The NH species was presumed to be the terminating molecule, whilst for the SF_6 plasma, peaks relating to F and SF were identified.

Initially, contact angle measurements were used to determine the ideal reaction times the samples should be run at in the reactor. For the SF_6 plasma, 20 s resulted in the most hydrophobic surface and was believed to give ideal coverage. Moreover, the decrease in contact angle suggested that damage may have occurred on the diamond surface after 20 s. For the NH_3 plasma, ideal surface coverage occurred after 120 s. There was no change in contact angle after this point and therefore it was believed that the ammonia plasma did not damage the surface.

XPS analysis showed the ammonia could be successfully deposited onto the diamond surface. It also showed that the H-termination used in the sample preparation was unstable and thus oxidized over time. This meant that the contact angle measurement may have been inaccurate as the surfaces were, in fact, a mixture of oxygen and nitrogen termination. The samples underwent the preparation process again and it was found that after 30 s there was a plateau in the amount of ammonia that could terminate the surface. This could be due to the steric constraints of the (100) surface. Additionally XPS data suggested that an increased exposure to the ammonia plasma results in a preference of imine groups on the diamond surface.

SEM analysis confirmed the suspicion that fluorine termination could etch the HPHT diamond surface. The etching was found to be varied across the diamond surface. Additionally, backscattered SEM showed the presence of another heavier atom on the carbon surface which was believed to be fluorine. However, without XPS analysis is impossible to confirm the atom's identity. SEM images also showed that etched areas still contained regions of possible fluorine termination.

Without XPS analysis of the SF_6 treated species, it is not possible to say definitively whether fluorine termination has taken place. However, given the contact angle measurements and SEM imaging it is likely that a successful termination was carried out. However, with the NH_3 -terminated samples we can definitively say that the reactor terminated the samples, however it did not result in a full monolayer of NH_3 -termination.

8. Further Work

As stated previously, XPS data would be needed to confirm the presence of F-termination on the diamond surface. Moreover, this would show us what percentage of a monolayer we could achieve with the reactor. The NanoESCA facility also allows for ultraviolet photoelectron spectroscopy (UPS) to be carried out. This will show how the electron affinity varies across the NH₃ and F terminated diamond surfaces.

Other groups have reported fluorine termination with other gases, such as CF₄ and XeF₂. The SF₆ gas can be easily exchanged in the reactor allowing for comparisons between all three gases. These other gases may have lower etching rates and allow for an increased exposure time, which in turn could allow for greater F-termination. Furthermore, other gases such as argon could be fed into the reactor at the same time to see if this has an effect on surface terminations and etching.

Additionally, the stability of both surfaces could be examined. This could be done by performing the initial termination reactions and then monitoring the change in monolayer coverage over time, to see if either the fluorine or ammonia surface is susceptible to oxidation.

Since the ammonia terminated samples contained both hydrogen and/or oxygen terminated regions, different preparation methods could be performed to see if a higher percentage of ammonia could be achieved. Other groups have found success by first terminating the diamond with chlorine and then ammonia. As the N-H molecule and Cl atom are similar in size it may result in easier substitutions on the surface.

In order to further confirm the presence of ammonia on the diamond surface, functionalization reactions could be performed, such as the attachment of biological molecules through amide linkages. Following this, the stability and functionality of the biological molecules on the diamond surface could be compared to their freely bound counterparts. This would give an indication on the biomedical uses of NH₃-terminated diamond.

Further research could look into the preference of imine groups on the diamond surface with an increased plasma exposure time. More samples should be run with varying plasma exposure time in order to get a better idea of the change in imine groups over time. Computational modelling could also be performed to see if the increased presence of imine groups allows for greater termination through surface rearrangements.

9. References

1. Bonke M. No Title. <http://www.michaelbonke.com/uploads/history-of-diamonds-en.pdf>. Published 2014.
2. USGS. *No Title.*; 2005. <https://minerals.usgs.gov/minerals/pubs/country/2005/myb3-2005-sf.pdf>.
3. Miyoshi Kazuhisa. *No Title*. Cleveland; 1998. <https://ntrs.nasa.gov/search.jsp?R=19980210770>.
4. Djemia P, Dugautier C, Chauveau T, Dogheche E, De Barros MI, Vandebulcke L. Mechanical properties of diamond films: A comparative study of polycrystalline and smooth fine-grained diamonds by Brillouin light scattering. *J Appl Phys*. 2001;90(8):3771-3779. doi:10.1063/1.1402667.
5. Mochalin VN, Shenderova O, Ho D, Gogotsi Y. The properties and applications of nanodiamonds. *Nat Nanotechnol*. 2011;7:11. <http://dx.doi.org/10.1038/nnano.2011.209>.
6. Zazula J. On Graphite Transformations at High Temperature and Pressure Induced by Absorption of the LHC Beam. *J Appl Phys*. 1997;78(1):433-476.
7. Martinez CA, Brillas E. *Synthetic Diamond Films: Preparation, Electrochemistry, Characterization, and Applications*. 1st ed. John Wiley and Sons; 2011.
8. Pal'yanov YN, Sokol AG, Borzdov YM, Khokhryakov AF, Sobolev N V. Diamond formation from mantle carbonate fluids. *Nature*. 1999;400:417. <http://dx.doi.org/10.1038/22678>.
9. Strong HM. Early diamond making at General Electric. *Am J Phys*. 1989;57(9):794-802. doi:10.1119/1.15895.
10. Taniguchi T. Synthesis of cubic diamond in the graphite-magnesium carbonate and graphite-K₂Mg(CO₃)₂ systems at high pressure of 9–10 GPa region. *J Mater Res*. 1996;11(10):2622-2631.
11. Kim JR, Zhu H, Pearson K. Step Heating For Growing High Quality Diamond. 2013:1-14.
12. Globe Newswire. Synthetic Diamonds Market Witnessing Strong Growth as Demand from End-Use Industries Rises - Global Industry Analysis, Size, Share, Growth, Trends and Forecast 2015 - 2023. NASDAQ.
13. Ullah M, Ahmed E, Hussain F, Rana AM, Raza R. Electrical conductivity enhancement by boron-doping in diamond using first principle calculations. *Appl Surf Sci*. 2015;334:40-44. doi:<https://doi.org/10.1016/j.apsusc.2014.07.157>.
14. Shigley J, Eaton S. Observations on CVD-Grown Synthetic Diamonds: A Review. *Gemological Inst Am*. 2016;52(3).
15. May PW. Diamond thin films: a 21st-century material. *Philos Trans R Soc London Ser A Math Phys Eng Sci*. 2000;358(1766):473 LP-495. <http://rsta.royalsocietypublishing.org/content/358/1766/473.abstract>.
16. Lee S-T, Lin Z, Jiang X. CVD diamond films: nucleation and growth. *Mater Sci Eng R Reports*. 1999;25(4):123-154. doi:[https://doi.org/10.1016/S0927-796X\(99\)00003-0](https://doi.org/10.1016/S0927-796X(99)00003-0).

17. Matsumoto S, Sato Y, Tsutsumi M, Setaka N. Growth of diamond particles from methane-hydrogen gas. *J Mater Sci*. 1982;17(11):3106-3112. doi:10.1007/BF01203472.
18. Spitsyn B V, Bouilov LL, Derjaguin B V. Vapor growth of diamond on diamond and other surfaces. *J Cryst Growth*. 1981;52(Part 1):219-226. doi:https://doi.org/10.1016/0022-0248(81)90197-4.
19. Goodwin DG, Gavillet GG. Numerical modeling of the filament-assisted diamond growth environment. *J Appl Phys*. 1990;68(12):6393-6400. doi:10.1063/1.346858.
20. D'Evelyn MP, Chu CJ, Hange RH, Margrave JL. Mechanism of diamond growth by chemical vapor deposition: Carbon-13 studies. *J Appl Phys*. 1992;71(3):1528-1530. doi:10.1063/1.351223.
21. Ma J, Cheesman A, Ashfold MNR, et al. Quantum cascade laser investigations of CH₄ and C₂H₂ interconversion in hydrocarbon/H₂ gas mixtures during microwave plasma enhanced chemical vapor deposition of diamond. *J Appl Phys*. 2009;106(3):33305. doi:10.1063/1.3176971.
22. Butler JE, Mankelevich YA, Cheesman A, Ma J, Ashfold MNR. Understanding the chemical vapor deposition of diamond: recent progress. *J Phys Condens Matter*. 2009;21(36):364201. doi:10.1088/0953-8984/21/36/364201.
23. Ashfold MNR, May PW, Petherbridge JR, et al. Unravelling aspects of the gas phase chemistry involved in diamond chemical vapour deposition. *Phys Chem Chem Phys*. 2001;3(17):3471-3485. doi:10.1039/B104265N.
24. Harris SJ, Belton DN. Thermochemical Kinetics of a Proposed Mechanism for Diamond Growth from Acetylene. *Jpn J Appl Phys*. 1991;30(Part 1, No. 10):2615-2618. doi:10.1143/JJAP.30.2615.
25. Bauer RA, Sbrockey NM, Brower WE. Quantitative nucleation and growth studies of PACVD diamond film formation on (100) silicon. *J Mater Res*. 1993;8(11):2858-2869. doi:DOI: 10.1557/JMR.1993.2858.
26. Macpherson J V. A practical guide to using boron doped diamond in electrochemical research. *Phys Chem Chem Phys*. 2015;17(5):2935-2949. doi:10.1039/C4CP04022H.
27. Chu CJ, D'Evelyn MP, Hauge RH, Margrave JL. Mechanism of diamond growth by chemical vapor deposition on diamond (100), (111), and (110) surfaces: Carbon-13 studies. *J Appl Phys*. 1991;70(3):1695-1705. doi:10.1063/1.349539.
28. Chu CJ, Hauge RH, Margrave JL, D'Evelyn MP. Growth kinetics of (100), (110), and (111) homoepitaxial diamond films. *Appl Phys Lett*. 1992;61(12):1393-1395. doi:10.1063/1.107548.
29. Petrini D, Larsson K. Origin of the Reactivity on the Nonterminated (100), (110), and (111) Diamond Surfaces: An Electronic Structure DFT Study. *J Phys Chem C*. 2008;112(37):14367-14376. doi:10.1021/jp711190r.
30. Scholze, Schmidt, Bechstedt. Structure of the diamond (111) surface: Single-dangling-bond versus triple-dangling-bond face. *Phys Rev B Condens Matter*. 1996;53(20):13725-13733.
31. Richley JC, Harvey JN, Ashfold MNR. CH₂ Group Migration between H-Terminated 2 × 1 Reconstructed {100} and {111} Surfaces of Diamond. *J Phys Chem C*. 2012;116(14):7810-7816. doi:10.1021/jp300454r.
32. Kern G, Hafner J, Kresse G. Atomic and electronic structure of diamond (111) surfaces I.

- Reconstruction and hydrogen-induced de-reconstruction of the one dangling-bond surface. *Surf Sci.* 1996;366(3):445-463. doi:[https://doi.org/10.1016/0039-6028\(96\)00837-0](https://doi.org/10.1016/0039-6028(96)00837-0).
33. Yu Y, Gu CZ, Xu LF, Zhang SB. Ab initio. *Phys Rev B.* 2004;70(12):125423. <https://link.aps.org/doi/10.1103/PhysRevB.70.125423>.
 34. Hong S, Chou MY. Theoretical study of hydrogen-covered diamond (100) surfaces: A chemical potential analysis. July 1996. doi:10.1103/PhysRevB.55.9975.
 35. Thomas ELH, Nelson GW, Mandal S, Foord JS, Williams OA. Chemical mechanical polishing of thin film diamond. *Carbon N Y.* 2014;68:473-479. doi:<https://doi.org/10.1016/j.carbon.2013.11.023>.
 36. Tran TTN, B. F, D. E, et al. Ultra-smooth single crystal diamond surfaces resulting from implantation and lift-off processes. *Phys status solidi.* 2011;208(9):2057-2061. doi:10.1002/pssa.201100038.
 37. Szunerits S, Boukherroub R. Different strategies for functionalization of diamond surfaces. *J Solid State Electrochem.* 2008;12(10):1205-1218. doi:10.1007/s10008-007-0473-3.
 38. Kawarada H. Hydrogen-terminated diamond surfaces and interfaces. *Surf Sci Rep.* 1996;26(7):205-259. doi:[https://doi.org/10.1016/S0167-5729\(97\)80002-7](https://doi.org/10.1016/S0167-5729(97)80002-7).
 39. Seshan V, Ullien D, Castellanos-Gomez A, et al. Hydrogen termination of CVD diamond films by high-temperature annealing at atmospheric pressure. *J Chem Phys.* 2013;138(23):234707. doi:10.1063/1.4810866.
 40. Williams OA, Jackman RB. Surface conductivity on hydrogen terminated diamond. *Semicond Sci Technol.* 2003;18(3):34-40.
 41. Koslowski B, Strobel S, Wenig MJ, Martschat R, Ziemann P. On the roughness of hydrogen-plasma treated diamond(100) surfaces. *Diam Relat Mater.* 1998;7(2):322-326. doi:[https://doi.org/10.1016/S0925-9635\(97\)00311-7](https://doi.org/10.1016/S0925-9635(97)00311-7).
 42. Hoffmann R, Kriele A, Obloh H, et al. Electrochemical hydrogen termination of boron-doped diamond. *Appl Phys Lett.* 2010;97(5):52103. doi:10.1063/1.3476346.
 43. Jin P, Maruno S. Bias Effect on the Microstructure and Diffusion Barrier Capability of Sputtered TiN and TiO_xN_y Films. *Jpn J Appl Phys.* 1992;31(Part 1, No. 5A):1446-1452. doi:10.1143/JJAP.31.1446.
 44. Albin S, Watkins L. Electrical properties of hydrogenated diamond. *Appl Phys Lett.* 1990;56(15):1454-1456. doi:10.1063/1.102496.
 45. Nemanich RJ, Carlisle JA, Hirata A, Haenen K. CVD diamond—Research, applications, and challenges. *MRS Bull.* 2014. doi:10.1557/mrs.2014.97.
 46. Landstrass MI, Ravi K V. Hydrogen passivation of electrically active defects in diamond. *Appl Phys Lett.* 1989;55(14):1391-1393. doi:10.1063/1.101604.
 47. Wort CJH, Balmer RS. Diamond as an electronic material. *Mater Today.* 2008;11(1):22-28. doi:[https://doi.org/10.1016/S1369-7021\(07\)70349-8](https://doi.org/10.1016/S1369-7021(07)70349-8).
 48. Krainisky IL, Asnin VM. Negative electron affinity mechanism for diamond surfaces. *Appl Phys Lett.* 1998;72(20):2574-2576. doi:10.1063/1.121422.
 49. May PW, Stone JC, Ashfold MNR, Hallam KR, Wang WN, Fox NA. The effect of diamond

- surface termination species upon field emission properties. *Diam Relat Mater.* 1998;7(2):671-676. doi:[https://doi.org/10.1016/S0925-9635\(97\)00181-7](https://doi.org/10.1016/S0925-9635(97)00181-7).
50. Shih A, Yater J, Pehrsson P, Butler J, Hor C, Abrams R. Secondary electron emission from diamond surfaces. *J Appl Phys.* 1997;82(4):1860-1867. doi:10.1063/1.365990.
 51. Ostrovskaya LY, Ral'chenko VG, Vlasov II, Khomich AA, Bol'shakov AP. Hydrophobic diamond films. *Prot Met Phys Chem Surfaces.* 2013;49(3):325-331. doi:10.1134/S2070205113030118.
 52. Mertens M, Mohr M, Brühne K, et al. Patterned hydrophobic and hydrophilic surfaces of ultra-smooth nanocrystalline diamond layers. *Appl Surf Sci.* 2016;390(Supplement C):526-530. doi:<https://doi.org/10.1016/j.apsusc.2016.08.130>.
 53. Sque SJ, Jones R, Briddon PR. Structure, electronics, and interaction of hydrogen and oxygen on diamond surfaces. *Phys Rev B.* 2006;73(8):85313. <https://link.aps.org/doi/10.1103/PhysRevB.73.085313>.
 54. Loh KP, Xie XN, Yang SW, Zheng JC. Oxygen Adsorption on (111)-Oriented Diamond: A Study with Ultraviolet Photoelectron Spectroscopy, Temperature-Programmed Desorption, and Periodic Density Functional Theory. *J Phys Chem B.* 2002;106(20):5230-5240. doi:10.1021/jp0139437.
 55. Klauser F, Ghodbane S, Boukherroub R, et al. Comparison of different oxidation techniques on single-crystal and nanocrystalline diamond surfaces. *Diam Relat Mater.* 2010;19(5):474-478. doi:<https://doi.org/10.1016/j.diamond.2009.11.013>.
 56. Krueger A. Chapter 8 - Current issues and challenges in surface chemistry of nanodiamonds A2 - Arnault, Jean-Charles BT - Nanodiamonds. In: *Micro and Nano Technologies.* Elsevier; 2017:183-242. doi:<https://doi.org/10.1016/B978-0-32-343029-6.00008-8>.
 57. Fink CK, Jenkins SJ. Ozonolysis of diamond. *J Phys Condens Matter.* 2009;21(26):264010. doi:10.1088/0953-8984/21/26/264010.
 58. Carbamates_Advances_in_Research_and_Appl.
 59. Popa E, Notsu H, Miwa T, Tryk D. Functionalization of the diamond surface. *Electrochem Solid State Lett.* 1999;2:49-51.
 60. Reed, P. B. *The Surface Chemistry of Diamond.*; 2014.
 61. Ando T, Yamamoto K, Matsuzawa M, et al. Direct interaction of elemental fluorine with diamond surfaces. *Diam Relat Mater.* 1996;5(9):1021-1025. doi:[https://doi.org/10.1016/0925-9635\(96\)00521-3](https://doi.org/10.1016/0925-9635(96)00521-3).
 62. Rutter MJ, Robertson J. Ab initio calculation of electron affinities of diamond surfaces. *Comput Mater Sci.* 1998;10(1):330-333. doi:[https://doi.org/10.1016/S0927-0256\(97\)00104-3](https://doi.org/10.1016/S0927-0256(97)00104-3).
 63. Fujishima A, Einaga Y, Narasinga T, Donald R, Tryk A. *Diamond Electrochemistry 1st Edition.* 1st ed. Amsterdam: Elsevier; 2005.
 64. Shirafuji J, Sugino T. Electrical properties of diamond surfaces. *Diam Relat Mater.* 1996;5(6):706-713. doi:[https://doi.org/10.1016/0925-9635\(95\)00415-7](https://doi.org/10.1016/0925-9635(95)00415-7).
 65. Salvadori MC, Araújo WWR, Teixeira FS, et al. Termination of diamond surfaces with hydrogen, oxygen and fluorine using a small, simple plasma gun. *Diam Relat Mater.* 2010;19(4):324-328. doi:<https://doi.org/10.1016/j.diamond.2010.01.002>.

66. Michalikova L, Rezek B, Kromka A, Kalbacova M. CVD diamond films with hydrophilic micro-patterns for self-organisation of human osteoblasts. *Vacuum*. 2009;84(1):61-64. doi:<https://doi.org/10.1016/j.vacuum.2009.04.016>.
67. Pederson M., Pickett WE. No Title. *Mater Res*. 1992;270(38).
68. Freedman A. Halogenation of diamond (100) and (111) surfaces by atomic beams. *J Appl Phys*. 1994;75(6):3112-3120. doi:10.1063/1.356163.
69. Nakamura T, Suzuki M, Ishihara M, Ohana T, Tanaka A, Koga Y. Photochemical Modification of Diamond Films: Introduction of Perfluorooctyl Functional Groups on Their Surface. *Langmuir*. 2004;20(14):5846-5849. doi:10.1021/la0499362.
70. Rietwyk KJ, Wong SL, Cao L, et al. Work function and electron affinity of the fluorine-terminated (100) diamond surface. *Appl Phys Lett*. 2013;102(9):91604. doi:10.1063/1.4793999.
71. Mayrhofer L, Moras G, Mulakaluri N, Rajagopalan S, Stevens PA, Moseler M. Fluorine-Terminated Diamond Surfaces as Dense Dipole Lattices: The Electrostatic Origin of Polar Hydrophobicity. *J Am Chem Soc*. 2016;138(12):4018-4028. doi:10.1021/jacs.5b04073.
72. Cui S, Hu EL. Increased negatively charged nitrogen-vacancy centers in fluorinated diamond. *Appl Phys Lett*. 2013;103(5):51603. doi:10.1063/1.4817651.
73. Acosta V, Hemmer P. Nitrogen-vacancy centers: Physics and applications. *MRS Bull*. 2013;38(2):127-130. doi:DOI: 10.1557/mrs.2013.18.
74. Doherty MW, Manson NB, Delaney P, Jelezko F, Wrachtrup J, Hollenberg LCL. The nitrogen-vacancy colour centre in diamond. *Phys Rep*. 2013;528(1):1-45. doi:<https://doi.org/10.1016/j.physrep.2013.02.001>.
75. Shintani Y, Kobayashi M, Kawarada H. An All-Solid-State pH Sensor Employing Fluorine-Terminated Polycrystalline Boron-Doped Diamond as a pH-Insensitive Solution-Gate Field-Effect Transistor. Seitz WR, ed. *Sensors (Basel)*. 2017;17(5):1040. doi:10.3390/s17051040.
76. Stacey A, O'Donnell KM, Chou J-P, et al. Nitrogen Terminated Diamond. *Adv Mater Interfaces*. 2015;2(10):1500079. doi:10.1002/admi.201500079.
77. Shellaiah M, Chen TH, Simon T, Li L-C, Sun KW, Ko F-H. An Affordable Wet Chemical Route to Grow Conducting Hybrid Graphite-Diamond Nanowires: Demonstration by A Single Nanowire Device. *Sci Rep*. 2017;7(1):11243. doi:10.1038/s41598-017-11741-9.
78. Chandran M, Shasha M, Michaelson S, Hoffman A. Nitrogen termination of single crystal (100) diamond surface by radio frequency N₂ plasma process: An in-situ x-ray photoemission spectroscopy and secondary electron emission studies. *Appl Phys Lett*. 2015;107(11):111602. doi:10.1063/1.4930945.
79. Wang Q, Kromka A, Houdkova J, et al. Nanomolar Hydrogen Peroxide Detection Using Horseradish Peroxidase Covalently Linked to Undoped Nanocrystalline Diamond Surfaces. *Langmuir*. 2012;28(1):587-592. doi:10.1021/la202967t.
80. Vizir A, Oks EM, Salvadori MC, Teixeira FS, Brown IG. Small plasma source for materials application. *Rev Sci Instrum*. 2007;78(8):86103. doi:10.1063/1.2766837.
81. Simon N, Charrier G, Gonçalves AM, et al. Direct amination of diamond surfaces by electroless treatment in liquid ammonia solution. *Electrochem Commun*. 2014;42(Supplement C):17-20. doi:<https://doi.org/10.1016/j.elecom.2014.01.024>.

82. Yang N, Uetsuka H, Watanabe H, Nakamura T, Nebel CE. Photochemical Amine Layer Formation on H-Terminated Single-Crystalline CVD Diamond. *Chem Mater*. 2007;19(11):2852-2859. doi:10.1021/cm070349m.
83. Takechi K, Lieberman MA. Effect of Ar addition to an O₂ plasma in an inductively coupled, traveling wave driven, large area plasma source: O₂/Ar mixture plasma modeling and photoresist etching. *J Appl Phys*. 2001;90(7):3205-3211. doi:10.1063/1.1398600.
84. Jee A-Y, Lee M. Surface functionalization and physicochemical characterization of diamond nanoparticles. *Curr Appl Phys*. 2009;9(2, Supplement):e144-e147. doi:https://doi.org/10.1016/j.cap.2008.12.045.
85. Nichols BM, Butler JE, Russell John N. J, Hamers RJ. Photochemical functionalization of hydrogen-terminated diamond surfaces: a structural and mechanistic study. *J Phys Chem B*. 2005;109(44):20938-20947.
86. Sund JB, Causey CP, Wolter SD, et al. Diamond surface functionalization with biomimicry – Amine surface tether and thiol moiety for electrochemical sensors. *Appl Surf Sci*. 2014;301(Supplement C):293-299. doi:https://doi.org/10.1016/j.apsusc.2014.02.067.
87. Li JS, Ueda E, Nallapaneni A, Li LX, Levkin PA. Printable Superhydrophilic–Superhydrophobic Micropatterns Based on Supported Lipid Layers. *Langmuir*. 2012;28(22):8286-8291. doi:10.1021/la3010932.
88. Mack Johnson. Microwave plasma-activated chemical vapour deposition of diamond: an investigation into Ncontaining plasmas. 2014.
89. Bird J. Studying the Oxidation of Diamond Using an O₂ Plasma Reactor. 2017.
90. Kimura T, Hanaki K. Probe Measurements and Optical Emission Spectroscopy in Inductively Coupled Ar/CF₄, Ar/NF₃, and Ar/SF₆ Discharges. *Jpn J Appl Phys*. 2008;47(11):8546-8552. doi:10.1143/JJAP.47.8546.
91. Christophorou LG, Olthoff JK. Electron Interactions With SF₆. *J Phys Chem Ref Data*. 2000;29(3):267-330. doi:10.1063/1.1288407.
92. Lamour G, Hamraoui A, Buvailo A, et al. Contact Angle Measurements Using a Simplified Experimental Setup. *J Chem Educ*. 2010;87(12):1403-1407. doi:10.1021/ed100468u.
93. Ihrig JL, Lai DYF. Contact angle measurement. *J Chem Educ*. 1957;34(4):196. doi:10.1021/ed034p196.
94. Griбанова E V, Zhukov AN, Antonyuk IE, Benndorf C, Baskova EN. Effect of the acidity of aqueous solutions on the wettability of diamond, graphite and pyrocarbon surfaces. *Diam Relat Mater*. 2000;9(1):1-6. doi:https://doi.org/10.1016/S0925-9635(99)00184-3.
95. Ostrovskaya L, Perevertailo V, Ralchenko V, Dementjev A, Loginova O. Wettability and surface energy of oxidized and hydrogen plasma-treated diamond films. *Diam Relat Mater*. 2002;11(3):845-850. doi:https://doi.org/10.1016/S0925-9635(01)00636-7.
96. Kruss. Young-Laplace fit. Kruss. <https://www.kruss-scientific.com/services/education-theory/glossary/young-laplace-fit/>. Published 2012.
97. Torrenго S, Minati L, Filippi M, et al. XPS and UPS investigation of the diamond surface oxidation by UV irradiation. *Diam Relat Mater*. 2009;18(5):804-807. doi:https://doi.org/10.1016/j.diamond.2009.02.003.

98. Juarez A. Introduction to hemispherical deflection analysers. ALAM Group. <http://es1.ph.man.ac.uk/research/facilities/IntroHDA.pdf>. Published 2013.
99. Saparin G V. Microcharacterization of CVD diamond films by scanning electron microscopy: morphology, structure and microdefects. *Diam Relat Mater.* 1994;3(11):1337-1351. doi:[https://doi.org/10.1016/0925-9635\(94\)90148-1](https://doi.org/10.1016/0925-9635(94)90148-1).
100. Kang SJ, Donnelly VM. Optical absorption and emission spectroscopy studies of ammonia-containing plasmas. *Plasma Sources Sci Technol.* 2007;16(2):265-272. doi:10.1088/0963-0252/16/2/008.
101. Navas J, Araujo D, Piñero JC, et al. Oxygen termination of homoepitaxial diamond surface by ozone and chemical methods: An experimental and theoretical perspective. *Appl Surf Sci.* 2018;433:408-418. doi:<https://doi.org/10.1016/j.apsusc.2017.10.065>.